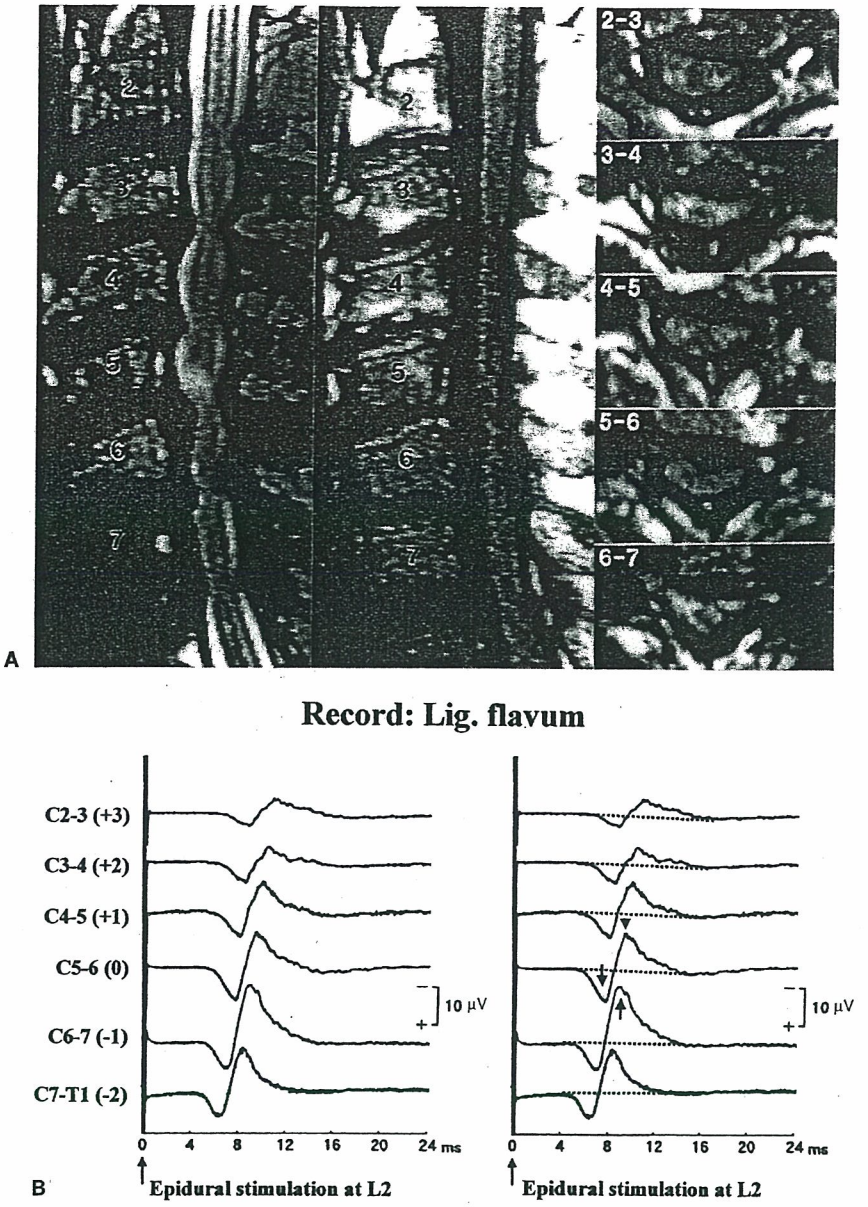

Fig. 3. (A) A sagittal T2-weighted MRI (TR 3636 ms; TE 96 ms) (left), and sagittal (middle), and axial (right) T1-weighted MRIs (TR 350 ms; TE 24 ms) in a 62-year-old man with cervical spondylotic myelopathy. Both the anteroposterior diameter and the cross-sectional area of the cord are smallest at C5–6, whereas a deformed cord is seen at C2–3 through C6–7. A high-intensity cord signal on T2-weighted image is also seen at C5–6. (B) Recording of EPs obtained from the same patient as in (A). The EPs were recorded unipolarly from the ligamentum flavum of C7–T1 through C2–3 after epidural stimulation at L2. The numerical label for each recording site is indicated on the left side. Drawing the baselines with dotted lines (right) helps identify conduction block. Note the increase in size of the negative peak (arrow pointing up) from C7–T1 (–2) to C6–7 (–1) followed by a reduction of the peak (arrow head) with a concomitant augmentation of the initial positive peak (arrow pointing down) at C5–6 (0).

TABLE 1

NEGATIVE PEAK OF EP

Recording level	Number of patients	Amplitude			Area		
		Mean (range) (μV)	Mean ± SD (%)	*p* value	Mean (range) (μV × ms)	Mean ± SD (%)	*p* value
+3	12	6.5 (0.7–29.5)	32 ± 15	NS	14.3 (0.3–55.2)	37 ± 22	NS
+2	27	5.4 (0.3–45.5)	31 ± 20	NS	11.0 (0.4–81.4)	32 ± 26	NS
+1	36	6.1 (0.4–33.0)	39 ± 24	NS	12.0 (0.1–50.7)	39 ± 32	NS
0	36	6.6 (0–42.9)	43 ± 21	<0.0001	11.3 (0–52.8)	37 ± 23	<0.0001
−1	36	16.4 (1.5–86.6)	100	NS	33.6 (3.9–120.0)	100	0.0135
−2	36	15.6 (1.3–86.6)	94 ± 17	NS	28.3 (3.4–110.6)	87 ± 19	0.011
−3	24	15.4 (0.9–73.2)	87 ± 20	NS	23.9 (1.7–88.4)	72 ± 21	NS
−4	11	12.4 (0.6–25.1)	84 ± 21		20.3 (1.1–40.5)	61 ± 22	

p values were based on the one-way analysis of variance followed by Fisher's PLSD test.

between two adjacent levels, in contrast to the initial positive component with a significant reduction in amplitude and area from "0" to "+1" and from "+1" to "+2" (Tables 1 and 2). In 27 patients who had EP recordings up to "+2" level, the negative component at "+1" or "+2" was significantly greater in area (42 ± 34% vs. 33 ± 24%; $p = 0.0198$), but not in amplitude, than at "0" (Fig. 2).

3.2. MRI

In the 36 patients with partial conduction block at single levels, sagittal and axial T1-weighted MRIs disclosed cord indentation at 78 levels and a deformed cord at 134 levels, respectively. Table 3 summarizes quantitative assessment of the cord compression in relation to the level of conduction block ("0" level). The "0" level always had both cord indentation and a deformed cord, showing a significantly smaller anteroposterior diameter ($p \leq 0.0002$) and cross-sectional area ($p \leq 0.0261$) of the cord compared to the remaining more caudal or rostral levels. However, the anteroposterior diameter or cross-sectional area of the cord was equally reduced or smaller at more caudal levels in 7 patients, at more rostral levels in 2, and at both more caudal and rostral levels in 4. Sagittal T2-weighted images disclosed high-intensity spinal cord signals at 27 levels in 22 patients. All matched the site of conduction block with the exception of five levels; two each located at "−1" and "−2" and one at "+1."

4. Discussion

Electrophysiological documentation of conduction block in chronic compression myelopathies plays an important role in elucidating the site responsible for the main functional change, particularly in the patients who have MRI evidence of multilevel compression (Tani et al., 1995). A conduction block in a single axon can be clearly identified by recording the action potential evoked in the nerve fiber. However, assessment of a spinal tract as a whole usually reveals more complicated features, because of the existence of interaction between potentials from constituent nerve fibers of different diameters. A major reduction in size of the compound sensory potential can result from physiologic desynchronization of the axonal volleys (Buchthal and Rosenfalck, 1966; Dorfman, 1984; Kimura et al., 1988). Thus, the evaluation of partial conduction block, as opposed to complete block, in the spinal cord, based on analysis of compound action potentials, requires careful exclusion of physiologic temporal dispersion that could substantially alter the waveform.

TABLE 2

POSITIVE PEAK OF EP

Recording level	Number of patients	Amplitude			Area			Latency		
		Mean (range) (μV)	Mean ± SD (%)	*p* value	Mean (range) (μV × ms)	Mean ± SD (%)	*p* value	Mean ± SD (ms)	Difference (ms)	*p* value
+3	12	4.1 (0.5–20.5)	47 ± 20	NS	4.2 (0.7–23.6)	73 ± 55	NS	6.78 ± 1.97	0.35 ± 0.11	
+2	27	3.8 (0.2–31.3)	73 ± 41	0.0018	5.1 (0.1–34.8)	122 ± 110	0.0301	7.08 ± 2.11	0.31 ± 0.14	NS
+1	36	5.7 (0.1–41.1)	122 ± 90	0.0004	8.8 (0.3–51.2)	264 ± 266	0.0214	6.81 ± 2.00	0.42 ± 0.29	NS
0	36	8.7 (0.5–45.1)	174 ± 95	<0.0001	16.2 (0.7–114.0)	403 ± 531	< 0.0001	6.39 ± 1.97	0.60 ± 0.36	0.0018
−1	36	6.1 (0.2–41.1)	100	NS	5.4 (0.1–34.0)	100	NS	5.79 ± 1.74	0.34 ± 0.13	< 0.0001
−2	36	6.6 (0.3–45.5)	110 ± 28	NS	5.4 (0.4–31.3)	118 ± 63	NS	5.45 ± 1.69	0.41 ± 0.16	NS
−3	24	7.7 (0.6–50.0)	131 ± 59	NS	6.6 (0.7–32.3)	155 ± 165	NS	5.22 ± 1.63	0.27 ± 0.09	NS
−4	11	6.3 (0.4–15.7)	151 ± 51		6.5 (0.6–21.0)	191 ± 151		4.65 ± 1.90		

p values were based on the one-way analysis of variance followed by Fisher's PLSD test.

TABLE 3

CERVICAL CORD MEASUREMENT

Intervertebral level	Number of patients	Anteroposterior diameter		Cross-sectional area	
		Mean ± SD	Range (mm)	Mean ± SD	Range (mm^2)
+3	10	6.2 ± 1.8	3.1–9.7	68.5 ± 19.9	41.7–99.2
+2	20	6.1 ± 1.5	3.8–9.5	70.7 ± 17.8	43.9–103.5
+1	30	5.7 ± 1.4	2.6–8.5	70.0 ± 17.3	25.9–95.5
0	36	4.0 ± 1.1*	1.7–6.2	51.2 ± 14.0*	17.3–77.6
−1	35	5.7 ± 1.0	3.8–7.8	64.8 ± 14.8	35.5–102.6
−2	26	5.9 ± 1.2	2.8–7.6	66.9 ± 13.3	39.9–92.7
−3	15	6.0 ± 0.7	4.8–7.2	64.4 ± 16.5	34.8–89.6

*Significantly smaller anteroposterior diameter ($p \leq 0.0002$) and cross-sectional area ($p \leq 0.0261$) of the cord than those at the remaining more caudal and rostral levels. p values were based on the one-way analysis of variance followed by Fisher's PLSD test.

The present study has shown that recording of ascending EPs in short increments helps identify a partial conduction block to localize a focal lesion. In surface recording at multiple levels for peripheral compressive neuropathies, the amplitude of nerve action potentials is greatly affected by the depth of the nerve from the skin surface. In contrast, intraoperative multisegmental recording registers comparable EPs, because all recording electrodes are nearly equidistant to the spinal cord if placed in the structures adjacent to the spinal cord such as ligamentum flavum. This technique can be carried out during surgery before decompression procedures.

We measured the positive and negative components of the EP separately to delineate the characteristic waveform changes of each component, which are affected differently. In this series of patients, the negative peak was significantly diminished at the site of conduction block compared to the immediately caudal level, although the degree of diminution ranged widely among different patients from a subtle (15%) to an extreme (100%) reduction in amplitude. With a subtle reduction of the negative peak, the presence of a concomitant enlargement of the initial positive peak or the incremental change of negative peaks caudal to that level, or both, distinguished partial conduction block from physiologic temporal dispersion. Without conduction block at the "0" level, the negative peak would have been progressively smaller in size from "–4" to "–1," as predicted from physiologic temporal dispersion. With an extreme reduction of the negative peak, its reappearance rostrally supported the diagnosis of partial, not complete, conduction block. The phenomenon of partial recovery of the negative peak beyond the site of conduction block was, although counter-intuitive, by no means the exception but the rule in partial conduction block. In fact, the area of the negative component was significantly greater either at "+1" or "+2" than at "0" in the patients who had EP recordings up to "+2" level.

A model using solid angle approximation (Woodbury, 1965; Brown, 1968; Tani et al., 1997; Kimura, 2001) and the concept of phase cancellation (Kimura et al., 1988; Kimura, 1998) can provide possible mechanisms that account for the above-mentioned waveform changes near the site of partial conduction block. The EP can be conceived of as a linear summation of potentials arising from constituent nerve fibers (Stegeman et al., 1979). If peaks of opposite polarity overlap, the EP will diminish in size because of phase cancellation (Kimura, 1988). At the site of conduction block, a blocked fiber contributes a normal

positivity followed by a substantially reduced negativity, as the impulse approaches without reaching the recording site. This reduction in negativity not only decreases the negative peak of EP but also increases its positive peak resulting from loss of physiologic phase cancellation. Thus, an enhancement of the initial positive EP peak indicates conduction block of fast-conducting fibers and that of the last positive EP peak, slow-conducting fibers (Ushida and Tani, 1994; Tani et al., 2001).

Immediately caudal to the site of conduction block, the impulse in a blocked fiber reaches the recording site giving rise to a normal negativity but does not move further away, failing to produce terminal positivity (Tani et al., 1998). Again, this reduction of positive phase enhances the negative peak of EP because of the loss of physiologic phase cancellation, accounting for the incremental change of the negative EP peaks.

The same consideration holds for the phenomenon that the negative peak partially recovers beyond the site of conduction block. Rostral to the site of conduction block, a blocked fiber gives rise to a killed-end effect with a volume-conducted positive wave, which quickly diminishes in size only a few centimeters away (Tani et al., 1997). A significant reduction in size of the initial positive EP component from "0" to "+1" and "+1" to "+2" reflects such a diminution of a killed-end effect. This steep reduction of positive wave from a blocked fiber rostral to conduction block can enhance the negative EP peak.

Electrophysiological abnormalities were consistent with MRI findings. The presence of partial conduction block implies a sufficient degree of cord compression, usually, but not always, at the level of the smallest anteroposterior diameter and cross-sectional area of the cord. However, there were intense but clinically silent compressions, as indicated by the lack of conduction block at these levels, in as many as 14 patients. In these cases, incremental EP studies are useful additions to MRI in localizing the primary site of cord involvement. Most high-intensity signals on sagittal T2-weighted MRIs corresponded to the site of partial conduction block. In the five exceptional levels, the discrepancy may have resulted from pathological changes of the cord segments with high-intensity signals confined to the gray matter (Al-Mefty et al., 1988).

5. Conclusions

Evaluation of the partial conduction block, as opposed to the complete block, requires careful exclusion of physiologic temporal dispersion. An enlargement of the initial positive peak at the site of conduction block together with the incremental change of the negative peak caudally helps identify partial conduction block, even though the negative peak reduction is small. Waveform changes useful in identifying a partial conduction block can be explained by the concept that a reduction in one polarity of constituent nerve fiber action potentials may eventually enhance the opposite polarity of the EP. An awareness of these changes near the site of partial conduction block should be helpful to localize a focal cord lesion, thus excluding clinically silent cord compression.

References

Al-Mefty, O., Harkey, L.H., Middleton, T.H., Smith, R.R. and Fox, J.L. (1988) Myelopathic cervical spondylotic lesions demonstrated by magnetic resonance imaging. *J. Neurosurg.*, 68: 217–222.

Brown, B.H. (1968) Theoretical and experimental waveform analysis of human compound nerve action potentials using surface electrodes. *Med. Biol. Eng.*, 6: 375–386.

Buchthal, F. and Rosenfalck, A. (1966) Evoked action potentials and conduction velocity in human sensory nerves. *Brain Res.*, 3: 1–122.

Cornblath, D.R., Sumner, A.J., Daube, J., Gilliat, R.W., Brown, W.F., Parry, G.J., Albers, J.W., Miller, R.G. and Petajan, J. (1991) Conduction block in clinical practice. *Muscle Nerve*, 14: 869–871.

Crandall, P.H. and Batzdorf, U. (1966) Cervical spondylotic myelopathy. *J. Neurosurg.*, 25: 57–66.

Deecke, L. and Tator, C.H. (1973) Neurophysiological assessment of afferent and efferent conduction in the injured spinal cord of monkeys. *J. Neurosurg.*, 39: 65–74.

Dorfman, L.J. (1984) The distribution of conduction velocities (DCV) in peripheral nerves: a review. *Muscle Nerve*, 7: 2–11.

Kimura, J. (1998) Kugelberg lecture: principles and pitfalls of nerve conduction studies. *Electroencephalogr. Clin. Neurophysiol.*, 106: 470–476.

Kimura, J. (2001) *Electrodiagnosis in Diseases of Nerve and Muscle: Principles and Practice,* Ed. 3. Oxford University Press, New York, pp. 27–38.

Kimura, J. and Kaji, R. (1991) Comment from the editorial office. *Muscle Nerve*, 14: 867–868.

Kimura, J., Sakimura, Y., Machida, M., Fuchigami, Y., Ishida, T., Claus, D., Kameyama, S., Nakazumi, Y., Wang, J. and Yamada, T. (1988) Effect of desynchronized input on compound sensory and muscle action potentials. *Muscle Nerve*, 11: 694–702.

Matsuda, H. and Shimazu, A. (1989) Intraoperative spinal cord monitoring using electric responses to stimulation of caudal spinal cord or motor cortex. In: J.E. Desmedt (Ed.), *Neuromonitoring in Surgery*. Elsevier, New York, pp. 175–190.

McDonald, W.I. and Sears, T.A. (1970) The effects of experimental demyelination on conduction in the central nervous system. *Brain*, 93: 583–598.

Nurick, S. (1972) The pathogenesis of the spinal cord disorder associated with cervical spondylosis. *Brain*, 95: 87–100.

Olney, R.K. and Miller, R.G. (1984) Conduction block in compression neuropathy: recognition and quantification. *Muscle Nerve*, 7: 662–667.

Ono, K., Ebara, S., Fuji, T., Yonenobu, K. and Fujiwara, K. (1987) Myelopathy hand; new clinical signs of cervical cord damage. *J. Bone Joint Surg.*, 69–B: 215–219.

Pelosi, L., Caruso, G. and Cracco, R.Q. (1991) Intraoperative recordings of spinal somatosensory evoked potentials to tibial nerve and sural nerve stimulation. *Muscle Nerve*, 14: 253–258.

Satomi, K., Okuma, T. and Kenmotsu, K. (1988) Level diagnosis of cervical myelopathy using evoked spinal cord potentials. *Spine*, 13: 1217–1224.

Schramm, J., Krause, R. and Shigeno, T. (1983) Experimental investigation on the spinal cord evoked injury potential. *J. Neurosurg.*, 59: 485–492.

Shimoji, K., Higashi H. and Kano, T. (1971) Epidural recording of spinal electrogram in man. *Electroencephalogr. Clin. Neurophysiol.*, 30: 236–239.

Stegeman, D.F., De Weerd, J.P.C. and Eijkman, E.G.J. (1979) A volume conductor study of compound action potentials of nerves in situ: the forward problem. *Biol. Cybern.*, 33: 97–111.

Takahashi, M., Yamashita, Y. and Sakamoto Y. (1989) Chronic cervical cord compression: clinical significance of increased signal intensity on MR images. *Radiology*, 173: 219–224.

Tamaki, T., Tsuji, H. and Inoue S. (1981) The prevention of iatrogenic spinal cord injury utilizing the evoked spinal cord potential. *Int. Orthop.*, 4: 313–317.

Tani, T., Ushida, T. and Yamamoto, H. (1995) Surgical treatment guided by spinal cord evoked potentials for tetraparesis due to cervical spondylosis. *Paraplegia*, 33: 354–358.

Tani, T., Ushida, T. and Yamamoto, H. (1997) Waveform changes due to conduction block and their underlying mechanism in spinal somatosensory evoked potential: a computer simulation. *J. Neurosurg.*, 86: 303–310.

Tani, T., Ushida, T. and Yamamoto, H. (1998) Waveform analysis of spinal somatosensory evoked potential: paradoxically enhanced negative peak immediately caudal to the site of conduction block. *Electroencephalogr. Clin. Neurophysiol.*, 108: 325–330.

Tani, T., Ushida, T. and Kimura, J. (2001) Sequential changes of orthodromic sensory nerve action potentials induced by experimental compression of the median nerve at the wrist. *Clin. Neurophysiol.*, 112: 136–144.

Ushida, T. and Tani, T. (1994) The spinal cord evoked potential by computer simulation: elucidation of killed-end potentials and augmentation caused by the conduction block phenomenon. *Nippon Seikeigeka Gakkai Zasshi (Jpn.)*, 68: 207–220.

Waxman, S.G., Kociss, J.D. and Black, J.A. (1995) Pathophysiology of demyelinated axons. In: S.G. Waxman, J.D. Kocsis and P.K. Stys (Eds.), *The Axon*. Oxford University Press, New York, pp. 438–461.

Woodbury, J.W. (1965) Potentials in a volume conductor. In: T.C. Ruch, H.D. Patton, J.W. Woodbury and A.L. Towe (Eds.), *Neurophysiology*, Ed. 2. Saunders, Philadelphia, PA, pp. 85–91.

REGULAR PAPER

J. Physiol. Sci. Vol. 56, No. 1; Feb. 2006; pp. 95–101
Online Feb. 25, 2006; **DOI: 10.2170/physiolsci.RP002305**

Nitric Oxide Stimulates Vascular Endothelial Growth Factor Production in Cardiomyocytes Involved in Angiogenesis

Masanori KUWABARA[1,2], Yoshihiko KAKINUMA[1], Motonori ANDO[1], Rajesh G. KATARE[1], Fumiyasu YAMASAKI[3], Yoshinori DOI[2], and Takayuki SATO[1]

[1]Department of Cardiovascular Control, Kochi Medical School, Nankoku, Japan; [2]Department of Medicine and Geriatrics, Kochi Medical School, Nankoku, Japan; and [3]Department of Clinical Laboratory, Kochi Medical School, Nankoku, Japan

Abstract: Background: Hypoxia-inducible factor (HIF)-1α regulates the transcription of lines of genes, including vascular endothelial growth factor (VEGF), a major gene responsible for angiogenesis. Several recent studies have demonstrated that a nonhypoxic pathway via nitric oxide (NO) is involved in the activation of HIF-1α. However, there is no direct evidence demonstrating the release of angiogenic factors by cardiomyocytes through the nonhypoxic induction pathway of HIF-1α in the heart. Therefore we assessed the effects of an NO donor, S-Nitroso-N-acetylpenicillamine (SNAP) on the induction of VEGF via HIF-1α under normoxia, using primary cultured rat cardiomyocytes (PRCMs). Methods and Results: PRCMs treated with acetylcholine (ACh) or SNAP exhibited a significant production of NO. SNAP activated the induction of HIF-1α protein expression in PRCMs during normoxia. Phosphatidylinositol 3-kinase (PI3K)–dependent Akt phosphorylation was induced by SNAP and was completely blocked by wortmannin, a PI3K inhibitor, and N^G-nitro-L-arginine methyl ester (L-NAME), a NO synthase inhibitor. The SNAP treatment also increased VEGF protein expression in PRCMs. Furthermore, conditioned medium derived from SNAP-treated cardiomyocytes phosphorylated the VEGF type–2 receptor (Flk-1) of human umbilical vein endothelial cells (a fourfold increase compared to the control group, $p < 0.001$, $n = 5$) and accelerated angiogenesis. Conclusion: Our results suggest that cardiomyocytes produce VEGF through a nonhypoxic HIF-1α induction pathway activated by NO, resulting in angiogenesis.

Key words: vascular endothelial growth factor, angiogenesis, cardiomyocyte, Flk-1, nitric oxide.

The prognosis of patients with chronic heart failure remains poor because of progressive remodeling of the heart and lethal arrhythmia [1]. It has recently been reported that vagal nerve stimulation therapy markedly improved long-term survival in an animal model of chronic heart failure after myocardial infarction [2] and that acetylcholine (ACh) has a direct cardioprotective effect through the PI3K-Akt-hypoxia-inducible factor (HIF)-1α pathway [3, 4]. Nitric oxide (NO) is supposed to be one of the signaling molecules induced by ACh; however, it remains to be clarified whether NO is involved in angiogenesis through the nonhypoxic induction pathway of HIF-1α and vascular endothelial growth factor (VEGF), and is thereby related to the cardioprotective effects of ACh or vagal nerve stimulation.

VEGF is a key angiogenic factor and major target of HIF-1α, which is produced by ischemic tissue and growing tumors [5–7]. Factors including VEGF secreted by noncardiomyocytes are known to possess significant paracrine effects on cardiomyocytes; however, the importance of such cardiomyocyte-derived factors as paracrine or autocrine effectors on angiogenesis in the heart remains to be elucidated. The HIF-1α protein level is usually regulated by the oxygen concentration. During hypoxia, HIF-1α protein is stabilized by escaping from degradation through von Hippel-Lindau tumor-suppressor protein (VHL) [8, 9]. Furthermore, the PI3K-Akt signaling pathway, which is known for the antiapoptotic functions [10, 11], is demonstrated to be involved in HIF-1α induction [12]. Recently it has been revealed that besides hypoxia, certain cytokines, growth factors, and NO increase the HIF-1α protein level even under the normoxic conditions in some specific cells [13–15]. To our knowledge, however, the involvement of NO in this signaling pathway in cardiomyocytes under normoxic conditions remains to be elucidated. Moreover, it is also unclear whether NO is involved in angiogenesis in the heart, though NO is associated with many aspects of cellular biology involved in cell signaling, vasodilatory tone, and cell growth [16].

With this background, we speculated the nonhypoxic induction of HIF-1α in the cardiomyocytes through NO-mediated pathway and that NO plays another role in producing an angiogenic factor through the pathway. To prove this hypothesis, we assessed the effect of a NO do-

Received on Dec 2, 2005; accepted on Feb 5, 2006; released online on Feb 25, 2006; DOI: 10.2170/physiolsci.RP002305
Correspondence should be addressed to: Yoshihiko Kakinuma, Department of Cardiovascular Control, Kochi Medical School, Nankoku, Kochi, 783-8505 Japan. Fax: +81-88-880-2310, Tel: +81-88-880-2587, E-mail: kakinuma@med.kochi-u.ac.jp

nor, *S*-Nitroso-*N*-acetylpenicillamine (SNAP), on the nonhypoxic induction of HIF-1α and the VEGF production in cardiomyocytes, using the primary cultured rat cardiomyocytes (PRCMs).

MATERIALS AND METHODS

Reagents. Reagents including the NO donor, *S*-nitroso-*N*-acetylpenicillamine (SNAP), acetylcholine (ACh), a phosphatidylinositol 3-kinase (PI3K) inhibitor, wortmannin, a specific nitric oxide synthase inhibitor, N^G-nitro-L-arginine methyl ester (L-NAME), and a transcriptional inhibitor, actinomycin D, were purchased from Sigma (Sigma Chemical Co., St. Louis, Missouri, USA).

Cell culture. This study followed the guidelines of the Council for Animal Care and was approved by an ethical committee of the Laboratory Animal Center, Kochi Medical School, Nankoku, Japan. According to the guideline, the Wistar rats used in this study were sacrificed. Primary cultured rat cardiomyocytes (PRCMs) were isolated from the hearts of 2-day-old neonatal rats and incubated on a gelatin-coated dish in DMEM/Ham F12 medium including 10% horse serum and ITS supplement according to our previous studies [17]. H9c2 cells have been frequently used to study the signal transductions and channels [18, 19]. H9c2 cells have been established as cell lines derived from the rat ventricular myocytes and thus far are widely used for many biological, biochemical, and electrophysiological studies because they have characteristics similar to PRCMs. Therefore they have often been utilized instead of PRCMs in studies where tons of rat cardiomyocytes are indispensable to perform experiments. To prepare many neonatal PRCMs for RNA isolation followed by RT-PCR, we used H9c2 cells, which, along with HEK 293, derived from human embryonic kidney cells, were incubated in DMEM supplemented with 10% FBS with antibiotics. To examine the effect of SNAP, cardiomyocytes in the serum-deficient medium were treated with either 1 μM (PRCMs, HEK 293 cells) or 1 mM (H9c2 cells) of SNAP.

Determination of NO from cardiomyocytes. To determine whether ACh and SNAP release NO in cardiomyocytes, we used an NO-sensitive fluorescent dye, diaminofluorescein-2 (DAF-2) (Daiichi Pure Chemicals Co. Ltd., Tokyo, Japan) [20]. PRCMs were treated with 10 μM DAF-2 and 100 μM L-arginine for 60 min, followed by 1 μM SNAP or 1 mM ACh. To examine the effect of L-NAME on NO production, the PRCMs were first pretreated with 1 mM L-NAME for 60 min, followed by the addition of DAF-2 and L-arginine. After incubation at 37°C, the cells were washed with PBS and observed under a fluorescence microscopy.

Western blotting analysis. To investigate the signal transduction pathway from SNAP to VEGF, we evaluated the effect of wortmannin (30 nM), actinomycin D (0.5 μg/ml), and L-NAME (1 mM) on Akt, HIF-1α, and VEGF by immunoblotting assay [21, 22]. Cardiomyocytes were pretreated with one of these agents prior to the addition of SNAP. After the incubation with SNAP, the cells were lysed and the total proteins isolated. The samples were then fractionated by 10% SDS-PAGE and transferred onto a PVDF membrane. Immunoblotting was performed with the primary antibodies against HIF-1α, VEGF (Santa Cruz Biotechnology, Santa Cruz, California, USA), Akt, phospho-Akt (Cell Signaling Technology, Beverly, Massachusetts, USA), or tubulin-α (Lab Vision, Fremont, California, USA), and was then reacted with an appropriate HRP-conjugated secondary antibody. The signal was detected with an enhanced chemiluminescence system (ECL Plus, Amersham, Piscataway, New Jersey, USA). Each experiment was performed in a duplicated fashion and repeated five times ($n = 5$), and representative data were shown.

Transfection. To investigate the direct contribution of HIF-1α to VEGF expression, HEK 293 cells were transfected with an expression vector for dominant-negative HIF-1α (dn HIF-1α) [23], using Effectene (Qiagen, Valencia, CA, USA) according to the manufacturer's protocol. HEK293 cells are derived from human embryonic kidney cells. It is known that the transient transfection of PRCMs with a conventional method is difficult and that the efficacy is extremely low. Compared with PRCMs, HEK293 cells have been extensively used for the transient transfection of an interested gene because of the extremely high efficiency of transfection and the higher protein expression level. Therefore we used HEK293 cells. Thirty-six hours after transfection, the HEK 293 cells were pretreated with 1 μM SNAP for 12 h, followed by an evaluation of the VEGF protein level. As a control, the cells were transfected with a vector for green fluorescent protein (GFP).

Reverse transcription-PCR (RT-PCR). RNA isolation and RT-PCR were performed as described earlier [17]. The synthesized cDNA was amplified with gene-specific primers for HIF-1α, VEGF, and Glut-1, as well as β-actin. The sense and antisense gene-specific primers were as follows:

HIF-1α (sense), 5'-GGGAGAAAAGCAAGTCGTG-3',
HIF-1α (antisense), 5'-AGTCAGCAACGTGGAAGG-3';
VEGF (sense), 5'-CCAGCACATAGGAGAGATGAGCTTC-3',
VEGF (antisense), 5'-GGTGTGGTGGTGACATGGTTAATC-3';
Glut-1 (sense), 5'-ACACCTCCCCCACATACATG-3',
Glut-1 (antisense), 5'-TGGAGTTTGGCTATAACACC-3';
β-actin (sense), 5'-GAAGATCCTGACCGAGCGTG-3',
β-actin (antisense), 5'-CGTACTCCTGCTTGCTGATCC-3'.

The optimal annealing temperature and the number of cycles for each template is as follows: 54°C, 30 cycles for HIF-1α; 62°C, 34 cycles for VEGF; 62°C, 36 cycles for Glut-1; and 60°C, 32 cycles for β-actin. PCR was performed in the range that gave a linear correlation between the amount of cDNA and the yield of PCR products. The

ratio of the RT-PCR product for each gene to that of β-actin was quantified and compared.

Immunohistochemistry. After SNAP treatment, H9c2 cells were fixed with 4% paraformaldehyde for 10 min and treated with 1% Triton X-100 for another 10 min. To block nonspecific antibody binding, the cells were incubated with 5% skim milk and successively incubated with a VEGF antibody (Santa Cruz Biotechnology, Santa Cruz, California, USA) in 1% skim milk at 4°C overnight and an FITC-labeled secondary antibody (Jackson ImmunoResearch Laboratories, West Grove, PA, USA) at 4°C overnight, then examined with an immunofluorescence microscope.

Human umbilical vein endothelial cells (HUVECs) culture. To understand if NO induces the cardiomyocytes to produce a factor responsible for angiogenesis, we examined the effect of conditioned medium derived from H9c2 cells treated with SNAP on HUVECs. The HUVECs were cultured in EGM-2 culture medium supplemented with angiogenic and growth factors (Cambrex Bio Science Walkersville, Inc., Walkersville, Maryland, USA). The H9c2 cells were treated with SNAP for 2 h and then incubated in the serum-free fresh medium. After 10 hours, the supernatant was collected and added to the HUVECs by replacing EGM-2 medium. The samples were collected before and after 60 min of stimulation with conditioned medium to evaluate the phosphorylation of VEGF receptor (Flk-1), using anti–pFlk-1 antibody (Santa Cruz Biotechnology, Santa Cruz, California, USA).

To further investigate the angiogenic effect of the conditioned medium derived from cardiomyocytes, the HUVECs were cultured on Matrigel (Becton Dickinson Labware, Bedford, Maryland, USA). The 96-well plates were coated with the diluted Matrigel (50 μl/well), incubated at 37°C for 1 h, then washed with serum-free DMEM. The HUVECs (1×10^4 cells) were seeded onto each well and cultured at 37°C for 10 h in DMEM, supplemented with 20% FBS, 25 μg/ml endothelial cell growth supplement (ECGS), 10 U/ml heparin, and conditioned medium derived from SNAP-treated or nontreated H9c2 cells.

Statistical analysis. Data are presented as mean ± SE. The differences were assessed by ANOVA followed by Fisher's PLSD for multiple comparisons. The results were considered statistically significant at $p < 0.05$.

RESULTS

A nonhypoxic induction of HIF-1α by NO through PI3K-Akt pathway

ACh or SNAP treatment rapidly increased the NO release in PRCMs within 30 min (Fig. 1); the release was continued and peaked at 8 h. In contrast, the cells pretreated with a nitric oxide synthase inhibitor L-NAME (1 mM) failed to show the NO signal (Fig. 1). The HIF-1α protein

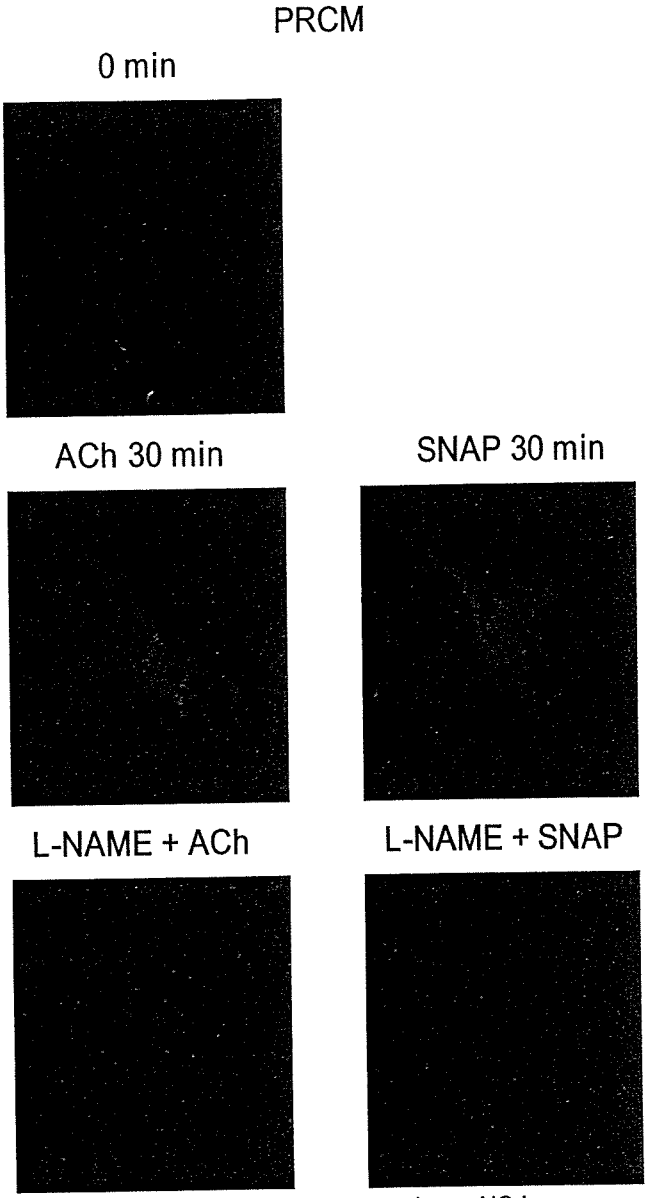

Fig. 1. Rat primary cardiomyocytes release NO in response to ACh or SNAP. PRCMs released NO after treatment with 1 mM ACh or 1 μM SNAP, evaluated with DAF-2. NO release was observed within 30 min after ACh or SNAP treatment ($n = 3$). Pretreatment with 1 mM L-NAME for 60 min blocked NO production ($n = 3$).

expression was gradually increased within 8 h since the SNAP treatment (a fivefold increase compared to the baseline (0 h), $p < 0.001$, $n = 5$) in PRCMs under normoxic conditions, thus confirming the occurrence of a nonhypoxic pathway for the HIF-1α induction in the cardiomyocytes (Fig. 2a). Such an induction of HIF-1α was also observed in H9c2 cells (data not shown). To understand if this induction is regulated at the transcriptional level, we pretreated cardiomyocytes with a commonly used transcriptional inhibitor, actinomycin D (0.5 μg/ml), followed by stimulation with SNAP for 8 h. However, actinomycin D failed to inhibit the HIF-1α induction by SNAP (Fig.

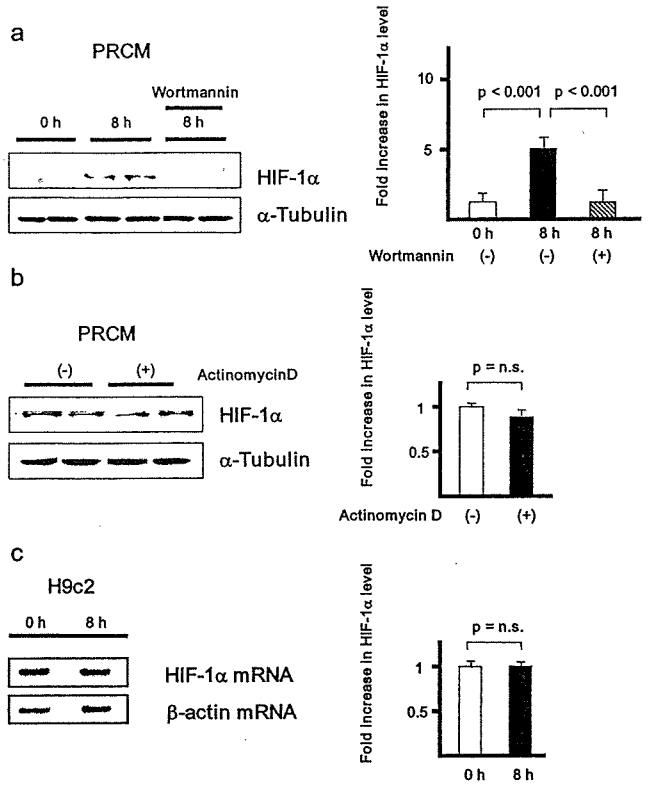

Fig. 2. The HIF-1α protein expression level is increased by SNAP in cardiomyocytes in normoxia. Treating the PRCMs for 8 h with SNAP (1 μM) already increased HIF-1α protein expression in normoxia. Pretreatment of PRCMs with wortmannin (30 nM) for 30 min inhibited SNAP-induced HIF-1α expression (n = 5) (**a**). However, treatment with actinomycin D (0.5 μg/ml) for 15 min did not inhibit the upregulation of HIF-1α protein expression by SNAP (n = 5) (**b**). In H9c2 cells, the HIF-1α mRNA expression level was not increased by SNAP (n = 5) (**c**).

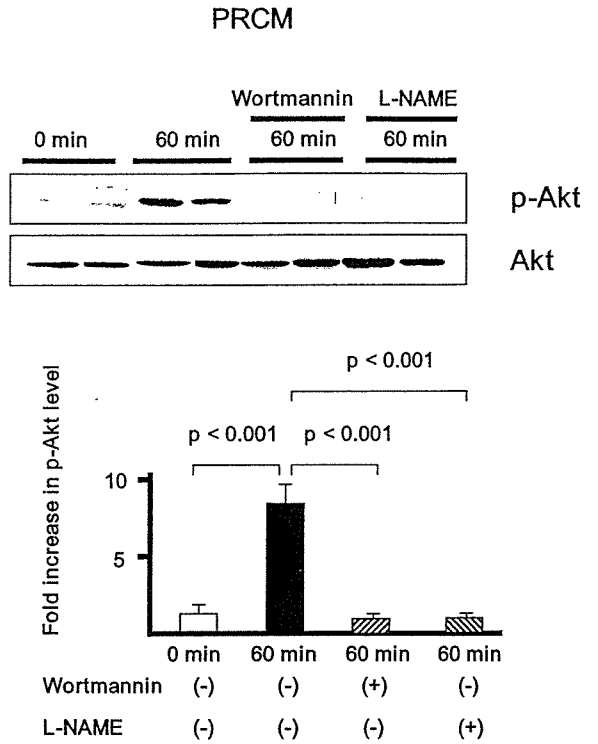

Fig. 3. Akt phosphorylation is increased by SNAP in cardiomyocytes under normoxia. Akt phosphorylation was increased by SNAP (1 μM) in PRCMs with a rapid time course. However, pretreatment with wortmannin (30 nM) for 60 min or L-NAME (1 mM) for 60 min completely inhibited the Akt phosphorylation in cardiomyocytes (n = 5).

2b), and SNAP further did not increase the HIF-1α mRNA level, evaluated by RT-PCR (Fig. 2c), thus suggesting that SNAP induces HIF-1α posttranslationally in normoxic conditions. Western blotting analysis further revealed an increased Akt phosphorylation with SNAP treatment for 60 min compared to the baseline (0 min) (an eightfold increase from the baseline, $p < 0.001$, $n = 5$) in PRCMs (Fig. 3). Pretreating the cells with PI3K inhibitor wortmannin (30 nM) or nitric oxide synthase inhibitor L-NAME (1 mM) prevented the SNAP-induced Akt phosphorylation (Fig. 3), thus demonstrating an important role for PI3K and NO in the Akt signaling pathway. Even though wortmannin (30 nM) was able to inhibit the SNAP-induced Akt or HIF-1α induction, it failed to block the NO release by the SNAP-treated cardiomyocytes (data not shown), thus confirming that NO remains upstream to the PI3K-Akt pathway. Moreover, these results also suggest the NO-dependent induction of HIF-1α in the cardiomyocytes under normoxic conditions.

Promotion of angiogenic signaling cascade by NO in cardiomyocytes under normoxia

To identify if SNAP-induced HIF-1α actually affects transcriptional activation of the target genes, the gene expression levels of the Glut-1 and VEGF were evaluated by the use of RT-PCR. The treatment of H9c2 cells with SNAP for 12 h under normoxic conditions increased the gene expressions of Glut-1 and VEGF, major HIF-1α–regulated genes (Fig. 4a). The protein expression level of VEGF was also increased following SNAP treatment, as demonstrated by the immunohistochemical and Western blotting analysis (Fig. 4 b and c). Consistent with the earlier findings, wortmannin was also able to inhibit the SNAP-induced VEGF expression in H9c2 cells and PRCMs (Fig. 4c), thus suggesting the PI3K-Akt mediated HIF-1α induction pathway in the production of VEGF by the cardiomyocytes under normoxic conditions. Furthermore, to elucidate the contribution of HIF-1α to VEGF protein expression, dn HIF-1α was introduced into HEK293 cells, and it was demonstrated that dn HIF-1α partially inhibits the VEGF induction by SNAP (Fig. 4d).

VEGF production in cardiomyocytes was further confirmed by an addition of conditioned medium derived from SNAP-treated or nontreated H9c2 cells to the HUVECs. As expected, the conditioned medium-treated cells

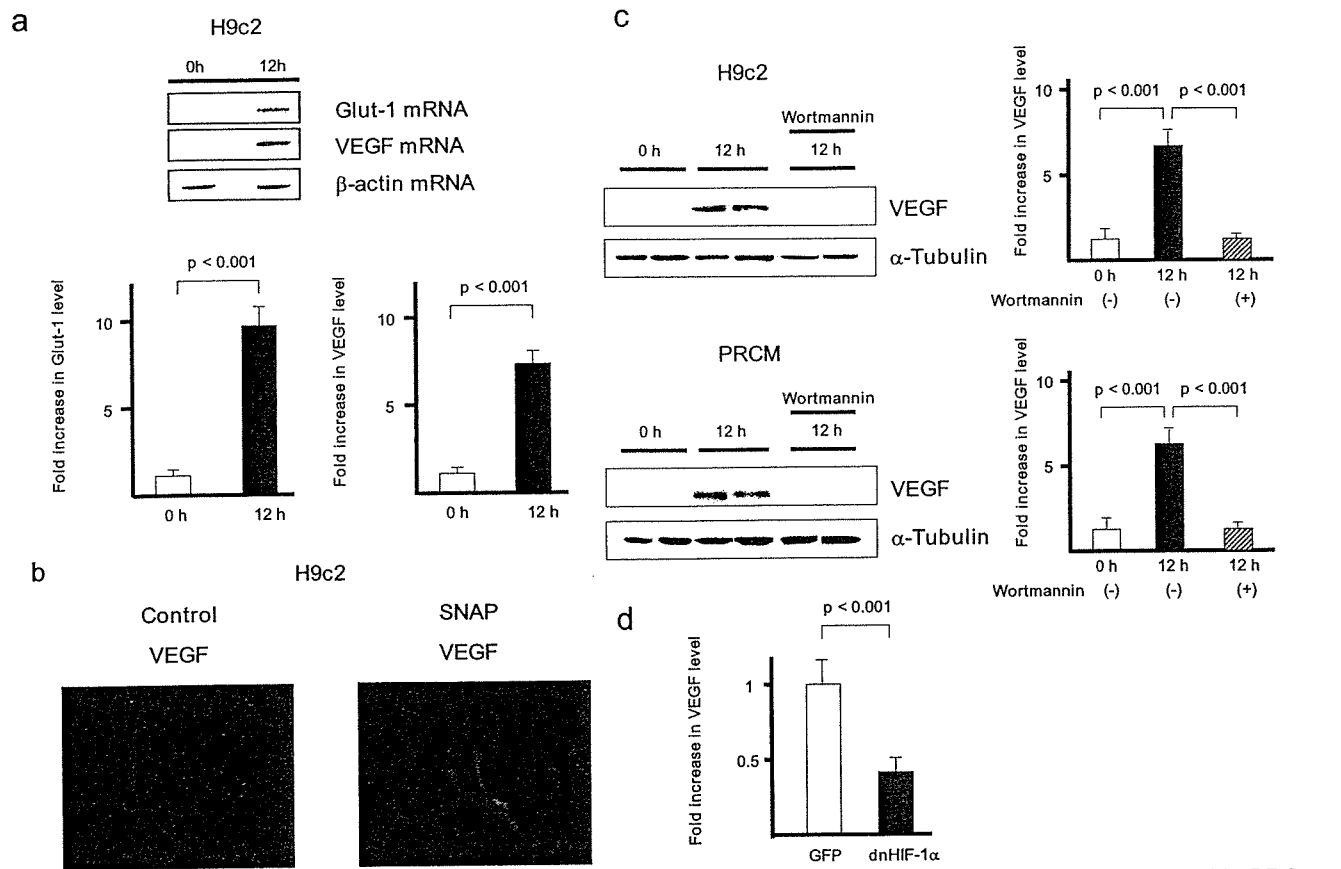

Fig. 4. SNAP increases Glut-1 and VEGF gene expression levels through HIF-1α in cardiomyocytes under normoxia. In H9c2 cells, Glut-1 mRNA and VEGF mRNA were both increased by SNAP ($n = 5$) (**a**). VEGF immunoreactivity was increased by SNAP in H9c2 cells ($n = 5$) (**b**). The SNAP-induced VEGF protein expression, which was also observed in PRCMs, was completely inhibited by 30 nM wortmannin ($n = 5$) (**c**). In contrast to control (GFP), VEGF induction by SNAP was blocked by dn HIF-1α in HEK293 cells ($n = 5$) (**d**).

(SNAP group) revealed increased Flk-1 phosphorylation (a fourfold increase compared to the control group, $p < 0.001$, $n = 5$), a VEGF type-2 receptor responsible for angiogenesis, in HUVECs (Fig. 5a). Furthermore, HUVECs were cultured on Matrigel in the presence of conditioned medium. Compared with the control group, the SNAP group activated more angiogenesis. It is suggested that SNAP exerts an acceleration of angiogenesis partially via cardiomyocyte-derived angiogenic factors, including VEGF (Fig. 5b).

DISCUSSION

It is well known that NO plays a critical role in modulating the vascular tone. According to the vascular effect, the depressed functional capacity of NO production would result in vasoconstriction and poor collateral circulation. Therefore NO or a NO donor has been used for coronary vasodilatation and decreasing blood pressure in systemic or pulmonary hypertension. However, the other effect of NO or a NO donor on cardiomyocytes remains to be fully investigated. It is known that NO is synthesized through eNOS in endothelial cells, and it is speculated that it has a significant paracrine effect on cardiomyocytes; however, it is unclear whether cardiomyocyte-derived NO possesses the direct action on cardiomyocytes to produce angiogenic factors.

Our previous study demonstrated the involvement of PI3K-Akt pathway in inducing the expression of HIF-1α by ACh during normoxia [4]. In the present study, SNAP-treated cardiomyocytes revealed a similar pathway in the induction of HIF-1α, suggesting that NO from cardiomyocytes activates an angiogenic signaling through HIF-1α.

As shown in the present study using DAF-2, a NO-sensitive dye, NO was detected in cardiomyocytes in response to SNAP as well as ACh, suggesting that cardiomyocytes release NO. The NO release by SNAP appeared in a rapid time course 30 min after the treatment, and it was not detected in PRCMs pretreated with L-NAME. Other studies have also reported the inhibitory effects of L-NAME on SNAP without the exact mechanisms being identified [24–27]; however, the speculated mechanism could be that the L-NAME pretreatment for 60 min of PRCMs might inhibit NO synthase, thereby reducing the basal NO production. Even if SNAP was thereafter added for 30 min to enhance NO release, the NO level in

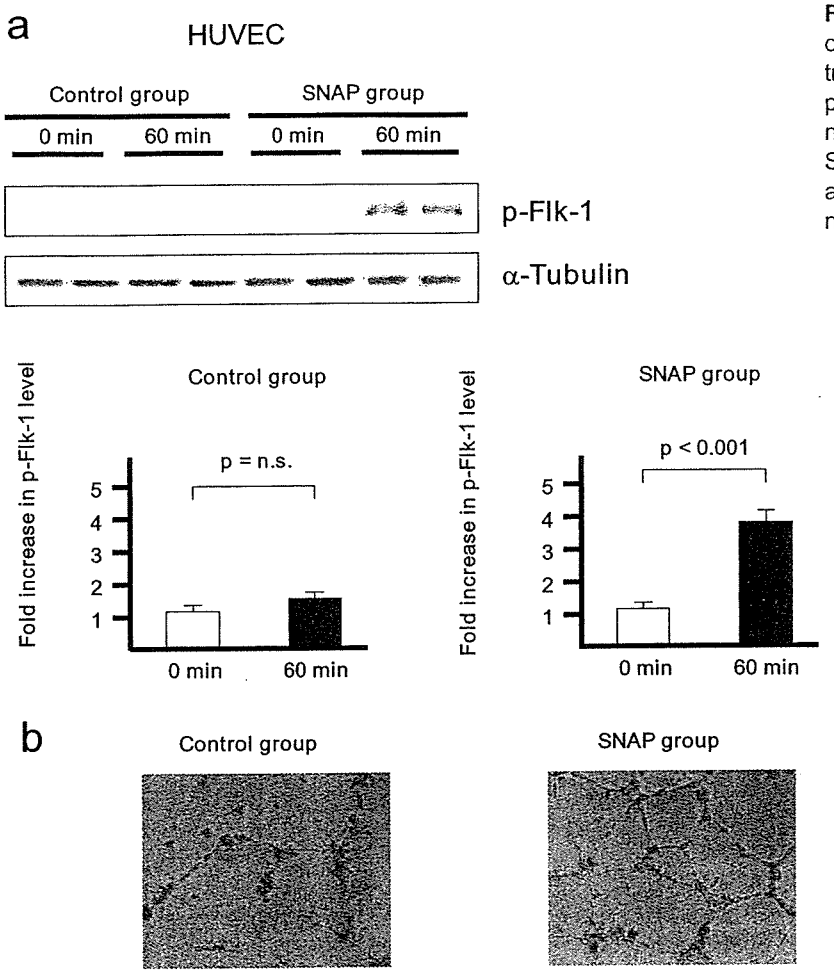

Fig. 5. VEGF derived from SNAP-treated cardiomyocytes induces angiogenesis. The SNAP-treated conditioned medium increased Flk-1 phosphorylation in HUVECs, compared with the nontreated conditioned medium (n = 5) (**a**). The SNAP-treated conditioned medium accelerated angiogenesis in HUVECs compared with the nontreated conditioned medium (**b**).

the treated cardiomyocyte might be too low, compared with the nontreated cell, to be detected by DAF-2. Therefore, these results suggest that cardiomyocyte-derived NO as a paracrine or autocrine effector plays a critical role in the HIF-1α induction in cardiomyocytes.

Second, as shown in this study, NO increased the cardiac VEGF protein expression through HIF-1α regulation, and dn HIF-1α decreased the VEGF expression by SNAP. VEGF itself has been reported to be involved in cell survival through the tyrosine kinase receptors, including VEGF type-2 receptor (Flk-1), activating Akt via a PI3K-dependent pathway [28], leading to eNOS upregulation. Furthermore, as suggested in our study, the cardiomyocyte-derived VEGF plays a crucial role in accelerating angiogenesis by endothelial cells in a paracrine fashion because VEGF produced by cardiomyocytes phosphorylated Flk-1 in HUVECs. These results suggest that cardiomyocytes can not only be a target for a NO donor to activate a nonhypoxic pathway of HIF-1α, but can also play a role in producing angiogenic factors in the heart. Taken together, the beneficial effects of NO might in part be a result of the cell signaling through PI3K-Akt, and also in part a result of the angiogenic signaling through HIF-1α–VEGF.

In the recent study by Giordano *et al.* [29], a cardiomyocyte-specific knockout of VEGF caused impaired cardiac development with hypovascularity in the heart, suggesting that cardiomyocyte-induced VEGF production is essential for cardiac development; however, their study did not reveal the precise cellular mechanism by which cardiac VEGF deletion leads to hypovasculature and depressed cardiac function. Our present study indicated that HIF-1α induction through NO plays a main role in stimulating VEGF production by cardiomyocytes and accelerates angiogenesis.

In this study we focused on HIF-1α as an upstream factor regulating cardiac VEGF expression. Unlike the hypoxic induction pathway of HIF-1α, there is no direct evidence for a nonhypoxic induction pathway of cardiomyocytes through NO involved in angiogenesis. Consequently, this study revealed another pathway of cardiac HIF-1α induction. PI3K-Akt signal has many aspects in cell survival, including an antiapoptotic activity, such as an inhibition of Bad-binding to Bcl-2 through Akt phosphorylation, an inhibition of proapoptotic caspases, including caspase 9 and Fas, and an inhibition of the activity of proapoptotic glycogen synthetase kinase-3 [30, 31]. In previous studies, which used other cell lines, the PI3K-

Akt pathway has been demonstrated to be involved in the NO-dependent stabilization of HIF-1α [14, 32–34]. As demonstrated in this study, in the presence of actinomycin D, the dose of which is adequate to inhibit transcriptional activity, SNAP posttranslationally regulated HIF-1α. Actinomycin D was used to identify which mechanisms are responsible for the increased protein expression, i.e., de novo synthesis or posttranslational modification. The protein level of HIF-1α was not decreased by actinomycin D; therefore this suggests that SNAP does not play a role in the transcriptional regulation of HIF-1α, rather in the inhibition of protein degradation. Therefore in cardiomyocytes, such a mechanism might be involved in a NO-mediated Akt-HIF-1α-VEGF signaling pathway, leading to cell protection.

In conclusion, it is suggested that NO has beneficial effects on cardiomyocytes by the activation of the nonhypoxic HIF-1α induction pathway, and furthermore, it contributes to angiogenesis through cardiac VEGF production, which phosphorylates Flk-1, a VEGF type-2 receptor.

This study was supported by a Health and Labor Sciences Research Grant (H15-PHYSI-001) for Advanced Medical Technology from the Ministry of Health, Labor, and Welfare of Japan.

REFERENCES

1. Julian DG, Gamm AJ, Frangin G, Janse MJ, Munoz A, Schwartz PJ, Simon P. Randomised trial of effect of amiodarone on mortality in patients with left-ventricular dysfunction after recent myocardial infarction: EMIAT. European Myocardial Infarct Amiodarone Trial Investigators. Lancet. 1997;349:667-74.
2. Li M, Zheng C, Sato T, Kawada T, Sugimachi M, Sunagawa K. Vagal nerve stimulation markedly improves long-term survival after chronic heart failure in rats. Circulation. 2004;109:120-4.
3. Krieg T, Qin Q, Philipp S, Alexeyev MF, Cohen MV, Downey JM. Acetylcholine and bradykinin trigger preconditioning in the heart through a pathway that includes Akt and NOS. Am J Physiol Heart Circ Physiol. 2004;287:H2606-11.
4. Kakinuma Y, Ando M, Kuwabara M, Rajesh G, Okudela K, Kobayashi M, Sato T. Acetylcholine from vagal stimulation protects cardiomyocytes against ischemic and hypoxia involving additive non-hypoxic condition of HIF-1α. FEBS Lett. 2005;579:2111-8.
5. Semenza GL. Hypoxia-inducible factor 1. oxygen homeostasis and disease pathophysiology. Trends Mol Med. 2001;7:345-50.
6. Ferrara N, Houck K, Jakeman L, Leung DW. Molecular and biological properties of the vascular endothelial growth factor family of proteins. Endocr Rev. 1992;13:18-32.
7. Wang GL, Jiang BH, Rue EA, Semenza GL. Hypoxia-inducible factor 1 is a basic-helix-loop-helix-PAS heterodimer regulated by cellular O_2 tension. Proc Natl Acad Sci USA. 1995;92:5510-4.
8. Maxwell PH, Wiesener MS, Chang GW, Clifford SC, Vaux EC, Cockman ME, Wykoff CC, Pugh CW, Maher ER, Ratcliffe PJ. The tumour suppressor protein VHL targets hypoxia-inducible factors for oxygen-dependent proteolysis. Nature. 1999;399:271-5.
9. Ivan M, Kondo K, Yang H, Kim W, Valiando J, Ohh M, Salic A, Asara JM, Lane WS, Kaelin Jr WG. HIF-1α targeted for VHL-mediated destruction by proline hydroxylation: Implications for O_2 sensing. Science. 2001;292:464-8.
10. Cantley LC, Auger KR, Carpenter C, Duckworth B, Graziani A, Kapeller R, Soltoff S. Oncogenes and signal transduction. Cell. 1991;64:281-302.
11. Yao R, Cooper GM. Requierment for phosphatidylinositol-3 kinase in the prevention of apoptosis by nerve growth factor. Science. 1995;267:2003-6.
12. Kandel ES, Hay N. The regulation and activities of the multifunctional serine/threonine kinase Akt/PKB. Exp Cell Res. 1999;253:210-29.
13. Richard DE, Berra E, Pouysségur J. Nonhypoxic pathway mediates the induction of hypoxia-inducible factor 1α in vascular smooth muscle cells. J Biol Chem. 2000;275:26765-71.
14. Sandau KB, Zhou J, Kietzmann T, Brune B. Regulation of the hypoxia-inducible factor 1 alpha by the inflammatory mediators nitric oxide and tumor necrosis factor-alpha in contrast to desferroxamine and phenylarsine oxide. J Biol Chem. 2001;276:39805-11.
15. Sandau KB, Fandrey J, Brune B. Accumulation of HIF-1alpha under the influence of nitric oxide. Blood. 2001;97:1009-15.
16. Balligand JL, Cannon PJ. Nitric oxide synthases and cardiac muscle: Autocrine and paracrine influences. Arterioscler Thromb Vasc Biol. 1997;17:1846-58.
17. Kakinuma Y, Miyauchi T, Yuki K, Murakoshi M, Goto K, Yamaguchi I. Novel molecular mechanism of increased myocardial endothelin-1 expression in the failing heart involving the transcriptional factor HIF-1α induced for impaired myocardial energy metabolism. Circulation. 2001; 103:2387-4.
18. Ilangovan G, Osinbowale S, Bratasz A, Bonar M, Cardounel AJ, Zweier JL, Kuppusamy P. Heat shock regulates the respiration of cardiac H9c2 cells through upregulation of nitric oxide synthase. Am J Physiol Cell Physiol. 2004;287:C1472-81.
19. Wu G, Mannam AP, Wu J, Kirbis S, Shie JL, Chen C, Laham RJ, Sellke FW, Li J. Hypoxia induces myocyte-dependent COX-2 regulation in endothelial cells: role of VEGF. Am J Physiol Heart Circ Physiol. 2003;285:H2420-H9.
20. Kimura C, Koyama T, Oike M, Ito Y. Hypotonic stress-induced NO production in endothelium depends on endogenous ATP. Biochem Biophys Res Commun. 2000;274:736-40.
21. Chachami G, Simos G, Hatziefthimiou A, Bonanou S, Molyvdas PA, Paraskeva E. Cobalt induces hypoxia-inducible factor-1alpha expression in airway smooth muscle cells by a reactive oxygen species and PI3K-dependent mechanism. Am J Respir Cell Mol Biol. 2004;31:544-51.
22. Weller R, Schwentker A, Billiar TR, Vodovotz Y. Autologous nitric oxide protects mouse and human keratinocytes from ultraviolet B radiation-induced apoptosis. Am J Physiol Cell Physiol. 2003;284:C1140-8.
23. Chen J, Zhao S, Nakada K, Kuge Y, Tamaki N, Okada F, Wang J, Shindo M, Higashino F, Takeda K, Asaka M, Katoh H, Sugiyama T, Hosokawa M, Kobayashi M. Dominant-negative hypoxia-inducible factor-1 alpha reduces tumorigenicity of pancreatic cancer cells through the suppression of glucose metabolism. Am J Pathol. 2004;162:1283-91.
24. Dang VC *et al.* Nitric oxide-cGMP-protein kinase G signaling pathway induces anoxic preconditioning through activation of ATP-sensitive K^+ channels in rat hearts. Am J Physiol Heart Circ Physiol. (Epub) Dec 9. 2005.
25. Chen J, Zhu JX, Wilson I, Cameron JS. Cardioprotective effects of K_{ATP} channel activation during hypoxia in goldfish carassius auratus. J Exp Biol. 2005;208:2765-72.
26. Maejima Y *et al.* Nitric oxide inhibits ischemia/reperfusion-induced myocardial apoptosis by modulating cyclin A-associated kinase activity. Cardiovasc Res. 2003;59:308-20.
27. Ebihara Y *et al.* Modulation of endothelin-a effects on rat hearts and cardiomyocytes by nitric oxide and 8-bromo cyclic GMP. J Mol Cell Cardiol. 1996;28:265-77.
29. Gerber HP, McMurtrey A, Kowalski J, Yan M, Kety BA, Dixit V, Ferrara N. Vascular endothelial growth factor regulates endothelial cell survival through the phosphatidyl-inositol 3'-kinase/Akt signal transduction pathway. Requirement for Flk-1/KDR activation. J Biol Chem. 1998;273:30336-43.
29. Giordano FJ, Gerber HP, Williams SP, VanBruggen N, Bunting S, Ruiz-Lozano P, Gu Y, Nath AK, Huang Y, Hickey R, Dalton N, Peterson KL, Ross J Jr, Chien KR, Ferrara N. A cardiac myocyte vascular endothelial growth factor paracrine pathway is required to maintain cardiac function. Proc Natl Acad Sci USA. 2001;98:5780-5.
30. Kennedy SG, Wagner AJ, Conzen SD, Jordan J, Bellacosa A, Tsichlis PN, Hay N. The PI3-kinase/Akt signaling pathway delivers an anti-apoptotic signal. Genes Dev. 1997;11:701-13.
31. Cross DA, Alessi DR, Cohen P, Andjelkovich M, Hemmings BA. Inhibition of glycogen synthase kinase-3 by insulin mediated by protein kinase B. Nature. 1995;378:785-9.
32. Kasuno K, Takabuchi S, Fukuda K, Kizaka-Kondoh S, Yodoi J, Adachi T, Semenza GL, Hirota K. Nitric oxide induces hypoxia-inducible factor 1 activation that is dependent on MAPK and phosphatidylinositol 3-kinase signaling. J Biol Chem. 2004;279:2550-8.
33. Sandau KB, Faus HG, Brune B. Induction of hypoxia-inducible-factor 1 by nitric oxide is mediated via the PI3K pathway. Biochem Biophys Res Commun. 2000;278:263-7.
34. Matzen E, Zhou J, Jelkmann W, Fandrey J, Brune B. Nitric oxide impairs normoxic degradation of HIF-1α by inhibition of prolyl hydroxylases. Mol Biol Cell. 2003;14:3470-81.

REGULAR PAPER

J. Physiol. Sci. Vol. 56, No. 3; Jun. 2006; pp. 235–245
Online Jul. 7, 2006; **doi:10.2170/physiolsci.RP006006**

Sympathetic Neural Regulation of Heart Rate Is Robust against High Plasma Catecholamines

Toru KAWADA[1], Tadayoshi MIYAMOTO[1,2], Yuichiro MIYOSHI[1], Sayo YAMAGUCHI[1], Yukiko TANABE[1], Atsunori KAMIYA[1], Toshiaki SHISHIDO[1], and Masaru SUGIMACHI[1]

[1]Department of Cardiovascular Dynamics, Advanced Medical Engineering Center, National Cardiovascular Center Research Institute, Osaka, 565-8565 Japan; and [2]Japan Association for the Advancement of Medical Equipment, Tokyo, 113-0033 Japan

Abstract: The sympathetic regulation of heart rate (HR) may be attained by neural and humoral factors. With respect to the humoral factor, plasma noradrenaline (NA) and adrenaline (Adr) can reportedly increase to levels approximately 10 times higher than resting level during severe exercise. Whether such high plasma NA or Adr interfered with the sympathetic neural regulation of HR remained unknown. We estimated the transfer function from cardiac sympathetic nerve stimulation (SNS) to HR in anesthetized and vagotomized rabbits. An intravenous administration of NA (n = 6) at 1 and 10 $\mu g \cdot kg^{-1} \cdot h^{-1}$ increased plasma NA concentration (pg/ml) from a baseline level of 438 ± 117 (mean ± SE) to 974 ± 106 and 6,830 ± 917 ($P < 0.01$), respectively. The dynamic gain (bpm/Hz) of the transfer function did not change significantly (from 7.6 ± 1.2 to 7.5 ± 1.1 and 8.1 ± 1.1), whereas mean HR (in bpm) during SNS slightly increased from 280 ± 24 to 289 ± 22 ($P < 0.01$) and 288 ± 22 ($P < 0.01$). The intravenous administration of Adr (n = 6) at 1 and 10 $\mu g \cdot kg^{-1} \cdot h^{-1}$ increased plasma Adr concentration (pg/ml) from a baseline level of 257 ± 86 to 659 ± 172 and 2,760 ± 590 ($P < 0.01$), respectively. Neither the dynamic gain (from 8.0 ± 0.6 to 8.4 ± 0.8 and 8.2 ± 1.0) nor the mean HR during SNS (from 274 ± 13 to 275 ± 13 and 274 ± 13) changed significantly. In contrast, the intravenous administration of isoproterenol (n = 6) at 10 $\mu g \cdot kg^{-1} \cdot h^{-1}$ significantly increased mean HR during SNS (from 278 ± 11 to 293 ± 9, $P < 0.01$) and blunted the transfer gain value at 0.0078 Hz (from 5.9 ± 1.0 to 1.0 ± 0.4, $P < 0.01$). In conclusion, high plasma NA or Adr hardly affected the dynamic sympathetic neural regulation of HR.

Key words: systems analysis, neuro-humoral interaction, noradrenaline, adrenaline, isoproterenol.

The sympathetic regulation of heart rate (HR) may be attained by neural and humoral factors. One unique feature of the neural regulation, which is in contrast to the humoral regulation, is its quickness. The quickness of regulation may be best quantified by identifying dynamic characteristics of the input-output or stimulus-response relationship of a given system [1, 2]. Although we have identified the dynamic characteristics of the HR regulation by the cardiac sympathetic nerve by using a transfer function analysis [3, 4], we ignored the possible effects of plasma catecholamines on the transfer function. Plasma concentrations of noradrenaline (NA) and adrenaline (Adr) can increase during systemic sympathetic activation. For instance, plasma NA and Adr both increase to approximately 10 times their respective resting levels during severe exercise [5]. They increase to approximately 6 and 20 times, respectively, during acute myocardial infarction [5]. Whether such high plasma NA or Adr interfered with the dynamic sympathetic neural regulation of HR remained unanswered.

Two mutually opposing hypotheses can be put forward regarding interactions between the humoral and neural factors in the sympathetic regulation of HR. The activation of presynaptic (or prejunctional) α_2-adrenergic receptors located on the postganglionic sympathetic nerve terminals inhibits NA release [6], which would result in the attenuated HR response to cardiac sympathetic nerve stimulation (SNS). In contrast, the activation of presynaptic (or prejunctional) β_2-adrenergic receptors located on the postganglionic sympathetic nerve terminals facilitates NA release [7], which would result in the augmented HR response to cardiac SNS. Besides these interactions, high plasma NA can increase the cardiac uptake of NA [8], which would modify the HR response to cardiac SNS.

The aim of the present study was to test the hypothesis that high plasma NA or Adr alters the dynamic sympathetic neural regulation of HR. Using anesthetized rabbits, we examined the HR response to random cardiac SNS under the condition of elevated plasma NA or Adr induced by exogenous administration. We also examined the effects of an intravenous administration of a β-adrenergic agonist isoproterenol on the HR response to SNS. The results of

Received on Jun 1, 2006; accepted on Jul 4, 2006; released online on Jul 7, 2006; doi:10.2170/physiolsci.RP006006
Correspondence should be addressed to: Toru Kawada, Department of Cardiovascular Dynamics, Advanced Medical Engineering Center, National Cardiovascular Center Research Institute, 5-7-1 Fujishirodai, Suita, Osaka, 565-8565 Japan. Phone: +81-6-6833-5012 (Ext. 2427), Fax: +81-6-6835-5403, E-mail: torukawa@res.ncvc.go.jp

the present study indicated that high plasma NA or Adr hardly affected the dynamic sympathetic neural regulation of HR in anesthetized rabbits.

MATERIALS AND METHODS

Animal preparation. The animals were cared for in strict accordance with the Guiding Principles for the Care and Use of Animals in the Field of Physiological Sciences approved by the Physiological Society of Japan. Eighteen Japanese white rabbits weighing from 2.4 to 3.2 kg were anesthetized by a mixture of α-chloralose (40 mg/ml) and urethane (250 mg/ml), initiated with a bolus injection of 2 ml/kg and maintained with a continuous administration at 0.5 $ml \cdot kg^{-1} \cdot h^{-1}$. The rabbits were intubated and mechanically ventilated with oxygen-enriched room air. The right cardiac postganglionic sympathetic nerve was identified in the right thoracic cavity and sectioned. Usually, HR dropped immediately after the sectioning of the right cardiac sympathetic nerve, suggesting the importance of the right cardiac sympathetic nerve in determining baseline HR. A pair of platinum electrodes was attached to the cardiac end of the sectioned nerve for stimulation. The nerve and electrodes were secured by silicone glue (Kwik-Sil, World Precision Instruments, Sarasota, FL, USA). The left cardiac sympathetic nerve and other sympathetic branches to the heart were kept intact. The carotid sinus nerves and aortic depressor nerves were sectioned bilaterally to minimize changes in systemic sympathetic activity induced by baroreflexes. The vagal nerves were also sectioned bilaterally to eliminate the vagal effect on the heart. The vagotomy did not change HR significantly at this stage, possibly because of the vagolitic effects of the anesthesia. Arterial pressure (AP) was measured by a micromanometer (Millar Instruments, Houston, TX, USA) inserted into the thoracic aorta from the right femoral artery. HR was measured with a cardiotachometer (AT-601G, Nihon Kohden, Tokyo, Japan). An arterial catheter was inserted into the left femoral artery to sample blood for plasma catecholamine measurements. A double-lumen venous catheter was introduced into the right femoral vein for continuous anesthetic infusion and exogenous catecholamine administration.

Protocols. We quantified the dynamic sympathetic neural regulation of HR by using a transfer function analysis [3, 4]. To estimate the transfer function from cardiac SNS to HR, we dynamically stimulated the right cardiac sympathetic nerve as follows. The pulse duration was set at 2 ms, and the pulse amplitude was adjusted to obtain an HR increase of approximately 50 bpm (beats/min) during a 5-Hz constant stimulation in each animal. The resulting amplitude ranged from 0.8 to 2.0 V among animals. With these settings, the stimulation frequency was randomly assigned at either 0 or 5 Hz every 2 s, according to a binary white noise sequence (see appendix A for additional information). The average stimulation frequency was therefore 2.5 Hz. The input power spectral density of SNS was relatively flat up to 0.25 Hz.

In *Protocol 1* ($n = 6$), physiological saline was infused intravenously at 1 $ml \cdot kg^{-1} \cdot h^{-1}$ for 30 min after the end of surgical preparation (Fig. 1). A 300-μl volume of arterial blood was sampled under control conditions (designated as NA_0 condition) for plasma catecholamine measurements. Following the blood sampling, dynamic SNS was applied for 15 min to estimate the transfer function from SNS to HR. Arterial blood was sampled during the last minute of dynamic SNS under the NA_0 condition. Next, 1-μg/ml NA solution was infused at 1 $\mu g \cdot kg^{-1} \cdot h^{-1}$ (NA_1). Fifteen min after the initiation of NA_1 administration, when AP and HR had reached new steady states, arterial blood sampling and 15-min dynamic SNS were repeated. Third, a 10-μg/ml NA solution was administered at 10 $\mu g \cdot kg^{-1} \cdot h^{-1}$ (NA_{10}). Fifteen min after the initiation of NA_{10} administration, arterial blood sampling and 15-min dynamic SNS were repeated.

In *Protocol 2* ($n = 6$), experimental procedures similar to those in *Protocol 1* were conducted, using the Adr solution instead of the NA solution. The transfer function from SNS to HR was estimated under control condition (designated as Adr_0 condition), as well as during the administration of 1-μg/ml Adr solution at 1 $\mu g \cdot kg^{-1} \cdot h^{-1}$ (Adr_1) and 10-μg/ml Adr solution at 10 $\mu g \cdot kg^{-1} \cdot h^{-1}$ (Adr_{10}).

In *Protocol 3* ($n = 6$), we examined the effects of an intravenous administration of a β-adrenergic agonist isoproterenol on the transfer function from SNS to HR. Using experimental procedures similar to those in *Protocol 1*, we

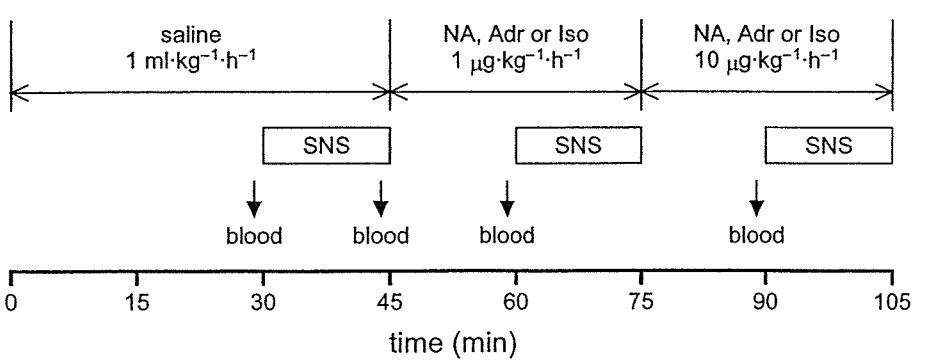

Fig. 1. Schematic diagram showing the experimental protocol. The downward arrows indicate the timings of blood sampling for catecholamine measurements (for *Protocols 1* and *2*). SNS: sympathetic nerve stimulation. NA: noradrenaline; Adr: adrenaline; Iso: isoproterenol.

administered 1-μg/ml isoproterenol solution at 1 μg·kg^{-1}·h^{-1} (Iso_1) and 10-μg/ml isoproterenol solution at 10 μg·kg^{-1}·h^{-1} (Iso_{10}) and estimated the transfer function under the control (designated as Iso_0), Iso_1, and Iso_{10} conditions.

Data analysis. The SNS command and HR were stored at a sampling rate of 200 Hz. The data were analyzed from only 2 min after the initiation of SNS to remove the initial trend of the HR increase. To estimate the transfer function from SNS to HR, we resampled the SNS-HR data pairs at 8 Hz. These data were segmented into 10 sets of half-overlapping bins of 1,024 data points each. In each segment, a linear trend was subtracted and a Hanning window was applied. The fast Fourier transform was then applied to obtain the frequency spectra of SNS and HR [9]. We calculated the ensemble averages of input power spectral density [$S_{SNS\cdot SNS}(f)$], output power spectral density [$S_{HR\cdot HR}(f)$], and cross-spectral density between the input and output [$S_{HR\cdot SNS}(f)$]. The transfer function [$H(f)$] was estimated using the following equation [10, 11].

$$H(f)=\frac{S_{HR\cdot SNS}(f)}{S_{SNS\cdot SNS}(f)} \tag{1}$$

We also calculated the magnitude-squared coherence function [$Coh(f)$] using the following equation [10, 11].

$$Coh(f)=\frac{\left|S_{HR\cdot SNS}(f)\right|^2}{S_{SNS\cdot SNS}(f)\,S_{HR\cdot HR}(f)} \tag{2}$$

The coherence function is a frequency-domain measure of the linear dependence between the input and output signals. A unity coherence value indicates a perfect linear dependence of HR on SNS, whereas a zero coherence value indicates the total independence between SNS and HR.

In *Protocols 1* and *2*, the transfer function from SNS to HR was parameterized by using a mathematical model [$H_m(f)$] of a second-order low-pass filter with pure dead time, using the following equation [3, 12].

$$H_m(f)=\frac{K}{1+2\zeta\frac{f}{f_N}j+\left(\frac{f}{f_N}j\right)^2}\exp(-2\pi f\,jL) \tag{3}$$

where K is the dynamic gain (in bpm/Hz), f_N is the natural frequency (in Hz), ζ is the damping ratio, and L is the pure dead time (in s); j represents the imaginary unit (see appendix B for details). A nonlinear iterative least square fitting was performed to minimize the following error function.

$$err=\frac{\sum_{i=1}^{N}\left|H(f_i)-H_m(f_i)\right|^2}{\sum_{i=1}^{N}\left|H(f_i)\right|^2},\quad f_i=f_0\times i \tag{4}$$

where f_0 indicates the fundamental frequency of the Fourier transform. N specifies the upper frequency bound of the fitting procedure. We set N at 32 so as to fit $H_m(f)$ to $H(f)$ up to 0.25 Hz.

In *Protocol 3*, because the transfer function from SNS to HR during Iso_{10} was significantly deviated from the mathematical model of a second-order low-pass filter with pure dead time (Eq. 3), we did not fit the mathematical model to the transfer function and adopted the transfer gain values at the lowest frequency ($G_{0.0078}$) and at 0.1 Hz ($G_{0.1}$) to represent the frequency response of HR to SNS.

Catecholamine measurements. The arterial blood sample was centrifuged and a 100-μl volume of plasma was obtained. The plasma was transferred into a 1.5-ml polypropylene conical tube. A 50-μl volume of the working internal standard solution [100 pg of 3,4-dihydroxybenzylamine (DHBA)], 5 mg of acid-washed alumina, and 1.0 ml of 1-M tris(hydroxymethyl) aminomethane buffer (pH 8.6), containing 0.2% disodium ethylendiaminetetraacetic acid (EDTA), was added to the conical tube and shaken for 15 min. After shaking, the alumina was washed three times with distilled water, transferred into a microfilter (Ultrafree C3, Millipore, Bedford, MA), and centrifuged to remove excess fluid. NA, Adr, and DHBA were then eluted from the alumina, using 60 μl of 2% acetic acid, and their concentrations were measured by using high-performance liquid chromatography with electrochemical detection (DTA-300, Eicom, Kyoto, Japan). Plasma NA and Adr concentrations were calculated, taking into account the recovery rate of DHBA.

Statistical analysis. All data are presented in mean and mean ± SEM values. In *Protocol 1*, the effect of dynamic SNS on the plasma NA concentration was examined by a paired *t*-test under NA_0 condition. The NA and Adr concentrations before SNS were compared among NA_0, NA_1, and NA_{10} conditions, using Dunnett's test against a single control following the repeated-measures analysis of variance [13]. We also compared mean HR, mean AP, and parameters of the transfer function among NA_0, NA_1, and NA_{10} conditions, using Dunnett's test following repeated-measures analysis of variance. In *Protocol 2*, the effect of dynamic SNS on the plasma Adr concentration was examined by a paired *t*-test under Adr_0 condition. Other values, including plasma NA and Adr concentrations, mean HR, mean AP, and parameters of the transfer function, were compared among Adr_0, Adr_1, and Adr_{10} conditions, using Dunnett's test following repeated-measures analysis of variance. In *Protocol 3*, mean HR, mean AP, and gain values ($G_{0.0078}$ and $G_{0.1}$) were compared among Iso_0, Iso_1,

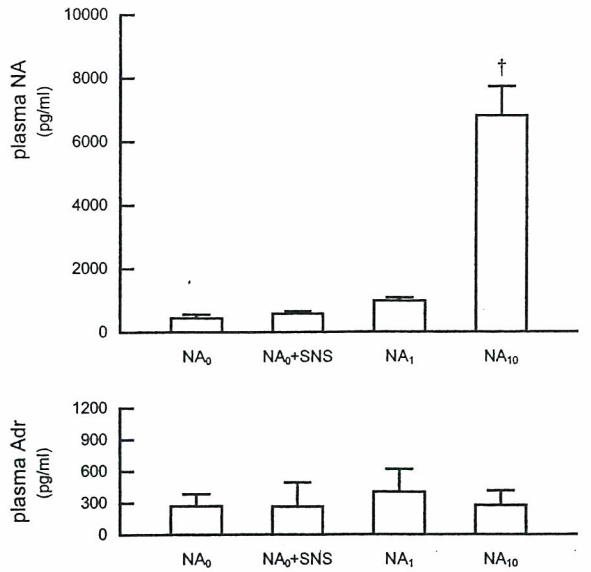

Fig. 2. Plasma concentrations of NA and Adr obtained from *Protocol 1*. The plasma NA concentration was significantly increased during the NA_{10} condition. The plasma Adr concentration was not changed significantly by the NA infusion. NA_0: saline infusion; NA_1 and NA_{10}: noradrenaline infusions at 1 and 10 $\mu g \cdot kg^{-1} \cdot h^{-1}$.

and Iso_{10} conditions, using Dunnett's test following repeated-measures analysis of variance. In all of the statistics, the difference was considered significant at $P < 0.05$.

RESULTS

Effects of high plasma NA on the dynamic sympathetic neural regulation of HR

In *Protocol 1*, dynamic SNS for 15 min did not change the plasma NA or Adr concentration significantly during NA_0 condition (Fig. 2, NA_0 vs. NA_0+SNS). The plasma NA concentration prior to dynamic SNS did not increase significantly during NA_1 condition, but increased to approximately 15 times higher during NA_{10} condition compared to NA_0 condition. The NA infusion did not significantly affect the plasma Adr concentration.

Figure 3A illustrates the time series of SNS, HR, and AP under NA_0, NA_1, and NA_{10} conditions obtained from one animal. The SNS was assigned at 0 or 5 Hz according to a binary white noise sequence. HR changed randomly in response to the dynamic SNS. Mean HR was slightly increased during NA infusion, whereas the amplitude of HR variation appeared unchanged. Mean AP was increased during NA_{10} condition compared to NA_0 condition.

Figure 3B shows averaged transfer functions from SNS to HR during NA_0, NA_1, and NA_{10} conditions obtained from all six animals in *Protocol 1*. The solid curve and the dashed curves in each plot represent mean and mean ± SEM values, respectively. In the gain plot, the transfer

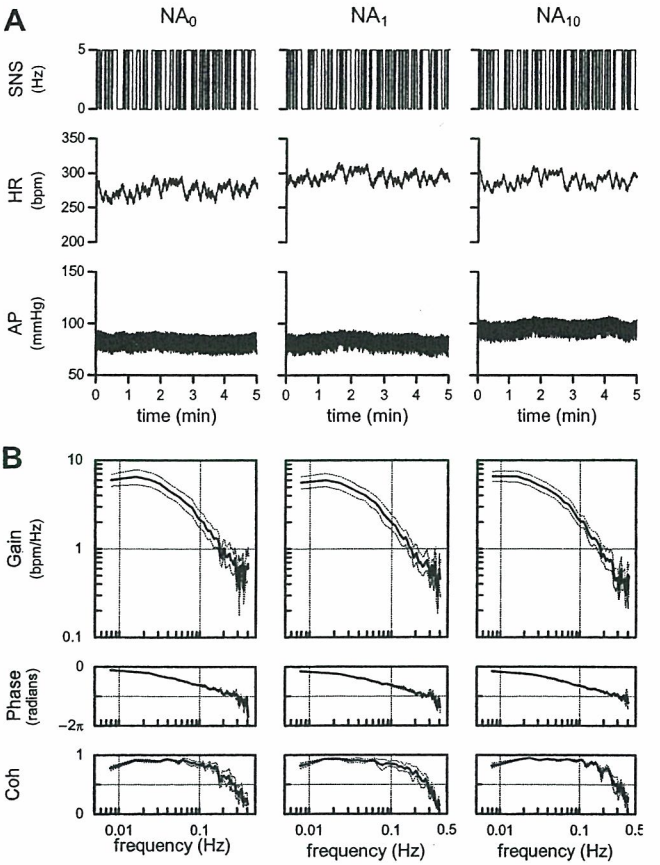

Fig. 3. A: Time series of one animal obtained from *Protocol 1*. Sympathetic nerve stimulation (SNS), heart rate (HR), and arterial pressure (AP) are shown. HR changed dynamically in response to SNS. **B**: Averaged transfer functions from SNS to HR during NA_0, NA_1, and NA_{10} conditions obtained from *Protocol 1* ($n = 6$). NA infusion did not affect the transfer function significantly except for changes in the damping ratio. Solid and dashed curves indicate mean and mean ± SEM values, respectively.

gain decreased with increasing frequency, reflecting the low-pass characteristics of the sympathetic neural regulation of HR. In the phase plot, the phase was near zero radians at the lowest frequency and delayed with increasing frequency, reflecting the SNS increases of HR. In the coherence plot, high coherence values up to 0.2 Hz indicate that approximately 80% of the HR variation in this frequency range was explained by the linear dynamics between SNS and HR. The transfer functions were similar among the three conditions. The dynamic gain, natural frequency, and pure dead time did not differ among the three conditions (Table 1). However, the damping ratio was significantly greater during NA_1 and NA_{10} conditions compared to the NA_0 condition.

Mean HR before SNS did not differ among NA_0, NA_1, and NA_{10} conditions, whereas mean HR during SNS increased significantly during NA_1 and NA_{10} conditions compared to NA_0 condition (Table 1). Although the repeated-measures analysis of variance indicated that the ef-

Table 1. Parameters obtained from *Protocol 1*.

	NA_0	NA_1	NA_{10}
HR, bpm			
Before SNS	248 ± 20	250 ± 19	251 ± 20
During SNS	280 ± 24	289 ± 22**	288 ± 22**
AP, mmHg			
Before SNS	95.7 ± 7.2	99.3 ± 8.1	106.6 ± 6.6*
During SNS	93.6 ± 8.0	102.9 ± 8.8**	106.0 ± 7.0**
Dynamic gain (K), bpm/Hz	7.6 ± 1.2	7.5 ± 1.1	8.1 ± 1.1
Natural frequency (f_N), Hz	0.080 ± 0.010	0.084 ± 0.010	0.083 ± 0.010
Damping ratio (ζ)	1.16 ± 0.05	1.48 ± 0.03*	1.52 ± 0.11*
Pure dead time (L), s	0.44 ± 0.08	0.55 ± 0.07	0.52 ± 0.06
Fitting error (err), %	1.6 ± 0.3	2.2 ± 0.6	1.6 ± 0.4

Values are means ± SEM. **$P < 0.01$ and *$P < 0.05$ vs. the corresponding value obtained during NA_0 condition. HR: heart rate. AP: arterial pressure. SNS: sympathetic nerve stimulation.

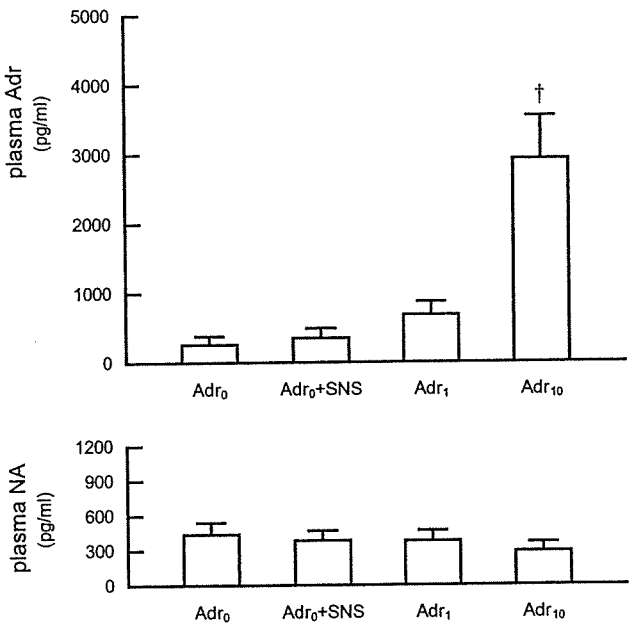

Fig. 4. Plasma concentrations of Adr and NA obtained from *Protocol 2*. The plasma Adr concentration was significantly increased during the Adr_{10} condition. The plasma NA concentration was not changed significantly by Adr infusion. Adr_0: saline infusion; Adr_1 and Adr_{10}: adrenaline infusions at 1 and 10 $\mu g \cdot kg^{-1} \cdot h^{-1}$.

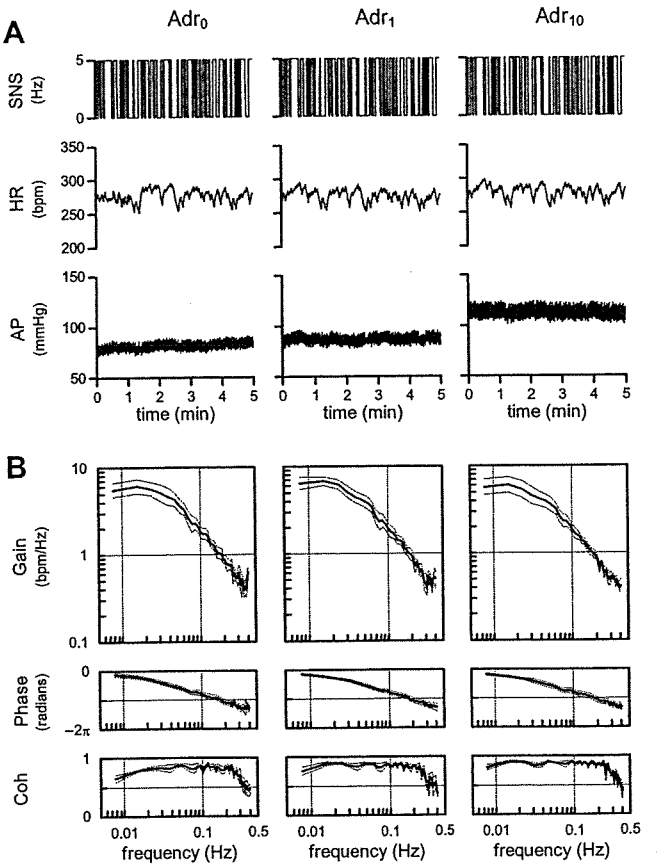

Fig. 5. A: Time series of one animal obtained from *Protocol 2*. HR changed dynamically in response to SNS. **B**: Averaged transfer functions from SNS to HR during Adr_0, Adr_1, and Adr_{10} conditions obtained from *Protocol 2* ($n = 6$). Adr infusion did not affect the transfer function significantly. Solid and dashed curves indicate mean and mean ± SEM values, respectively.

fects of NA infusion on mean HR during SNS were significant, the magnitude of the HR increase was small relative to the interindividual variation of HR. Mean AP before SNS was significantly elevated during NA_{10} condition, but not during NA_1 condition compared to NA_0 condition. Mean AP during SNS was increased significantly during both NA_1 and NA_{10} conditions compared to NA_0 condition.

Table 2. Parameters obtained from *Protocol 2*.

	Adr_0	Adr_1	Adr_{10}
HR, bpm			
Before SNS	231 ± 12	232 ± 10	228 ± 7
During SNS	274 ± 13	275 ± 13	274 ± 13
AP, mmHg			
Before SNS	93.1 ± 9.7	99.0 ± 8.3	113.7 ± 5.2**
During SNS	101.3 ± 8.0	103.8 ± 8.4	116.6 ± 4.6**
Dynamic gain (K), bpm/Hz	8.0 ± 0.6	8.4 ± 0.8	8.2 ± 1.0
Natural frequency (f_N), Hz	0.070 ± 0.005	0.071 ± 0.005	0.067 ± 0.006
Damping ratio (ζ)	1.09 ± 0.20	1.32 ± 0.11	1.39 ± 0.17
Pure dead time (L), s	0.55 ± 0.13	0.66 ± 0.09	0.63 ± 0.15
Fitting error (err), %	2.5 ± 0.5	1.8 ± 0.3	2.3 ± 0.6

Values are means ± SEM. **$P < 0.01$ vs. the corresponding value obtained during Adr_0 condition. HR: heart rate. AP: arterial pressure. SNS: sympathetic nerve stimulation.

Effects of high plasma Adr on the dynamic sympathetic neural regulation of HR

In *Protocol 2*, dynamic SNS for 15 min did not significantly change the plasma Adr or NA concentration during Adr_0 condition (Fig. 4, Adr_0 vs. Adr_0+SNS). The plasma Adr concentration prior to dynamic SNS did not increase significantly during Adr_1 condition, but increased to approximately 11 times higher during Adr_{10} condition compared to Adr_0 condition. The Adr infusion did not significantly affect the plasma NA concentration.

Figure 5A illustrates the time series of SNS, HR, and AP during Adr_0, Adr_1, and Adr_{10} conditions obtained from one animal. HR changed randomly in response to the dynamic SNS. The Adr infusion did not significantly change mean HR or the amplitude of HR variation among Adr_0, Adr_1, and Adr_{10} conditions. Mean AP increased during Adr_{10} condition compared to the Adr_0 condition.

Figure 5B shows averaged transfer functions from SNS to HR during Adr_0, Adr_1, and Adr_{10} conditions obtained from all of the six animals in *Protocol 2*. There seem to be no effects of Adr infusion on the transfer functions. No significant differences in dynamic gain, natural frequency, damping ratio, and pure dead time were observed among the three conditions (Table 2).

Mean HR did not differ significantly among Adr_0, Adr_1, and Adr_{10} conditions, both before and during SNS (Table 2). Mean AP increased significantly during Adr_{10} condition, but not during Adr_1 condition compared with Adr_0 condition, both before and during SNS.

Effects of intravenous isoproterenol on the dynamic sympathetic neural regulation of HR

Figure 6A illustrates the time series of SNS, HR, and AP during Iso_0, Iso_1, and Iso_{10} conditions obtained from one animal. HR changed randomly in response to the dynamic SNS under the Iso_0 condition. Although the dynamic HR response to SNS was maintained under the Iso_1 condition, mean HR was significantly elevated, and no apparent HR response was observed under the Iso_{10} condition.

Figure 6B shows averaged transfer functions from SNS to HR during Iso_0, Iso_1, and Iso_{10} conditions obtained from all of the six animals in *Protocol 3*. The transfer function showed a slight downward shift under the Iso_1 condition compared to the Iso_0 condition. It was significantly deformed and lost consistent characteristics across the animals under the Iso_{10} condition, as evidenced by large standard errors (dashed lines). The gain values ($G_{0.0078}$ and $G_{0.1}$) were significantly lower under the Iso_{10} condition compared to the Iso_0 condition (Table 3).

Mean HR did not change significantly under the Iso_1 condition, but increased significantly under the Iso_{10} condition compared to that under the Iso_0 condition, both before and during SNS (Table 3). Mean AP before SNS was significantly increased under the Iso_1 condition, but not under the Iso_{10} condition compared to that under the Iso_0 condition. Mean AP during SNS did not differ under the Iso_1 condition, but decreased significantly under the Iso_{10} condition compared to that under the Iso_0 condition.

DISCUSSION

We have examined the effects of high plasma NA or Adr on the transfer function from SNS to HR and found that high plasma catecholamines within physiological limits (approximately 10 times the resting levels) were ineffective to alter the sympathetic neural regulation of HR. Although the baseline HR was higher than the resting HR reported in conscious rabbits, the high baseline HR may be partly due to vagotomy. Because dynamic SNS (average stimulation frequency was 2.5 Hz) could increase mean HR, on the average, by 32 bpm in *Protocol 1* and by 43 bpm in *Protocol 2* under control conditions (NA_0 and Adr_0), the insignificant effects of high plasma catecholamines on HR cannot be explained by a simple saturation

Table 3. Parameters obtained from *Protocol 3*.

	Iso_0	Iso_1	Iso_{10}
HR, bpm			
Before SNS	244 ± 7	245 ± 6	289 ± 8**
During SNS	278 ± 11	280 ± 10	293 ± 9**
AP, mmHg			
Before SNS	80.2 ± 8.5	96.2 ± 4.9*	83.5 ± 7.1
During SNS	90.9 ± 7.4	93.1 ± 7.4	82.9 ± 7.0**
$G_{0.0078}$, bpm/Hz	5.9 ± 1.0	4.7 ± 0.8	1.0 ± 0.4**
$G_{0.1}$, bpm/Hz	1.3 ± 0.3	0.9 ± 0.2	0.2 ± 0.2**

Values are means ± SEM. $^{**}P < 0.01$ and $^{*}P < 0.05$ vs. the corresponding value obtained during Iso_0 condition. HR: heart rate. AP: arterial pressure. SNS: sympathetic nerve stimulation. $G_{0.0078}$: transfer gain value at 0.0078 Hz. $G_{0.1}$: transfer gain value at 0.1 Hz.

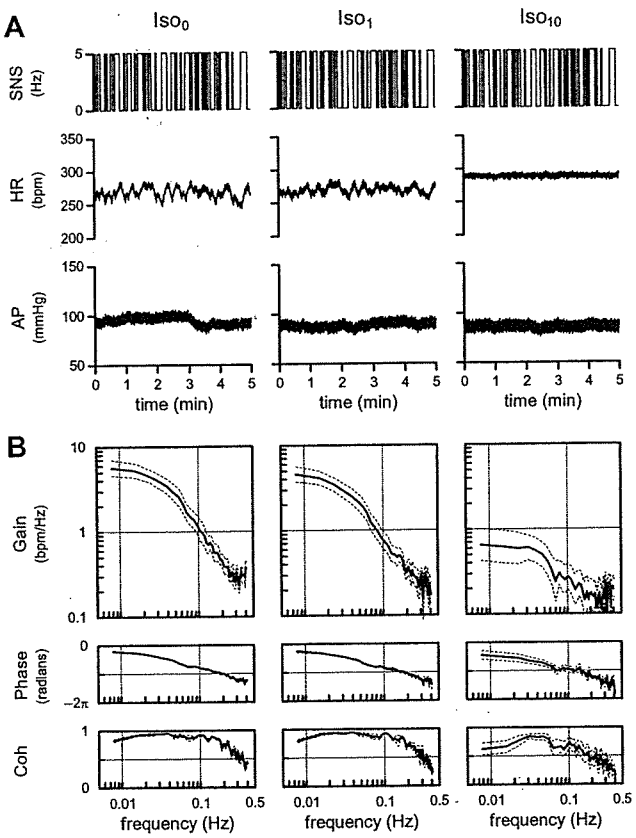

Fig. 6. A: Time series of one animal obtained from *Protocol 3*. Although HR changed dynamically in response to SNS under Iso_0 and Iso_1 conditions, mean HR elevated significantly, and no apparent dynamic HR response was observed under the Iso_{10} condition. **B**: Averaged transfer functions from SNS to HR during Iso_0, Iso_1, and Iso_{10} conditions obtained from *Protocol 3* (n = 6). The transfer gain reduced significantly and varied among animals, as evidenced by the large SEM under the Iso_{10} condition. Solid and dashed curves indicate mean and mean ± SEM values, respectively. Iso_0: saline infusion; Iso_1 and Iso_{10}: isoproterenol infusions at 1 and 10 $\mu g \cdot kg^{-1} \cdot h^{-1}$.

phenomenon of the HR response to catecholamines or by complete downregulation of β-adrenergic receptors under the present experimental settings. Actually, we confirmed that the same dose of intravenous administration of a β-adrenergic agonist isoproterenol increased mean HR significantly and blunted the transfer function (Fig. 6, Iso_{10} in *Protocol 3*). It is quite likely that NA released from the sympathetic nerve terminals during SNS has much stronger effects on HR in comparison with circulating catecholamines.

Effects of high plasma NA on the sympathetic neural regulation of HR

The plasma NA concentration increased approximately 15 times higher during NA_{10} condition than during NA_0 condition. Nevertheless, mean HR before SNS did not change significantly during NA_{10} condition compared to NA_0 condition (Table 1). In contrast, mean AP before SNS increased significantly during NA_{10} condition compared to NA_0 condition (Table 1). Young *et al.* [14] also reported an increase in AP and no changes in HR during NA infusion at 0.2 $\mu g \cdot kg^{-1} \cdot min^{-1}$ (12 $\mu g \cdot kg^{-1} \cdot h^{-1}$) in conscious dogs, though the baroreflexes could have counteracted the potential increase of HR in their study. These results indicate that the vascular bed is more responsive to plasma NA than the sinus node. A tighter synaptic cleft of the neuroeffector junction of the cardiac muscle compared to the vasculature, though it was reported in rat tissues [15], might explain the differential sensitivity to plasma NA between HR and AP.

Cardiac SNS significantly increased the mean HR without increasing the plasma NA concentration (Fig. 2), consistent with previous studies in anesthetized dogs [16] and cats [17]. Although mean HR before SNS did not differ among NA_0, NA_1, and NA_{10} conditions, mean HR during SNS was significantly higher during NA_1 and NA_{10} conditions compared to control (Table 1). These results are in opposition to the hypothesis that high plasma NA activates presynaptic α_2-adrenergic receptors and attenuates the HR response to SNS. One possible explanation for the increased mean HR during SNS under conditions of the NA infusion is as follows. NA released from the sympathetic nerve terminals is removed from the synaptic cleft by two catecholamine uptake mechanisms: a high-affinity, low-capacity neuronal uptake ($uptake_1$) and a low-affinity, high-capacity extraneuronal uptake ($uptake_2$) [5,